Downloaded from rsta.royalsocietypublishing.org on August 12, 2013

PHILOSOPHICAL TRANSACTIONS OF THE ROYAL SOCIETY A MATHEMATICAL, PHYSICAL & ENGINEERING SCIENCES

Spectroscopy of light-molecule endofullerenes

Malcolm H. Levitt

Phil. Trans. R. Soc. A 2013 **371**, 20120429, published 5 August 2013

References

This article cites 96 articles, 11 of which can be accessed free
http://rsta.royalsocietypublishing.org/content/371/1998/20120429.full.html#ref-list-1

Subject collections

Articles on similar topics can be found in the following collections

photochemistry (18 articles)
physical chemistry (36 articles)
spectroscopy (42 articles)
supramolecular chemistry (9 articles)
synthetic chemistry (5 articles)

Email alerting service

Receive free email alerts when new articles cite this article - sign up in the box at the top right-hand corner of the article or click **here**

To subscribe to *Phil. Trans. R. Soc. A* go to:
http://rsta.royalsocietypublishing.org/subscriptions

Downloaded from rsta.royalsocietypublishing.org on August 12, 2013

PHILOSOPHICAL TRANSACTIONS OF THE ROYAL SOCIETY A

rsta.royalsocietypublishing.org

Review

Cite this article: Levitt MH. 2013 Spectroscopy of light-molecule endofullerenes. Phil Trans R Soc A 371: 20120429.
http://dx.doi.org/10.1098/rsta.2012.0429

One contribution of 13 to a Theo Murphy Meeting Issue 'Nanolaboratories: physics and chemistry of small-molecule endofullerenes'.

Subject Areas:
physical chemistry, spectroscopy, supramolecular chemistry, photochemistry, synthetic chemistry

Keywords:
endofullerenes, spin isomers, parahydrogen, neutron scattering, nuclear magnetic resonance, infrared spectroscopy

Author for correspondence:
Malcolm H. Levitt
e-mail: mhl@soton.ac.uk

Royal Society Publishing
Informing the science of the future

Spectroscopy of light-molecule endofullerenes

Malcolm H. Levitt

School of Chemistry, University of Southampton, Highfield, Southampton SO17 1BJ, UK

Molecular endofullerenes are supramolecular systems consisting of fullerene cages encapsulating small molecules. Although most early examples consist of encapsulated metal clusters, recently developed synthetic routes have provided endofullerenes with non-metallic guest molecules in high purity and macroscopic quantities. The encapsulated light molecule behaves as a confined quantum rotor, displaying rotational quantization as well as translational quantization, and a rich coupling between the translational and rotational degrees of freedom. Furthermore, many encapsulated molecules display spin isomerism. Spectroscopies such as inelastic neutron scattering, nuclear magnetic resonance and infrared spectroscopy may be used to obtain information on the quantized energy level structure and spin isomerism of the guest molecules. It is also possible to study the influence of the guest molecules on the cages, and to explore the communication between the guest molecules and the molecular environment outside the cage.

1. Introduction

Fullerenes consist of closed carbon cages containing exactly 12 pentagons. The revolutionary discovery of these new carbon allotropes by Kroto *et al*. [1] initiated the field of carbon nanomaterials, which has impacted on a wide range of physical sciences. The exterior surface of the fullerenes may be subjected to numerous chemical reactions, and the closed interior surface may encapsulate atoms and molecules, generating the supramolecular species known as endofullerenes [2]. The notation A@C_n has been widely adopted, where A is the encapsulated atom or molecule and n is the number of carbons in the fullerene cage [2].

The first reported endofullerene was La@C_{82}. This substance was generated by laser vaporization of a lanthanum oxide/graphite composite [2]. Species are also formed with multiple metal atoms trapped inside

© 2013 The Author(s) Published by the Royal Society. All rights reserved.

Downloaded from rsta.royalsocietypublishing.org on August 12, 2013

the fullerene cavity [2]. A wide range of metallo-endofullerenes have now been characterized [3–7]. Many of these substances have endohedral guest clusters consisting of one or more metal atoms, and sometimes non-metals as well. A seminal example is $Sc_3N@C_{80}$ in which a cluster of four atoms is trapped inside a C_{80} cage [6].

Fullerenes are usually synthesized by arc discharge, which involves the high-temperature vaporization of carbon [8]. Metallo-endofullerenes are generated by vaporizing metals at the same time as the carbon, so that the metal atoms or clusters are captured as the carbon cages form. Some non-metallic endofullerenes may also be synthesized in this way. For example, small quantities of atomic endofullerenes such as $He@C_{60}$ and $Ne@C_{60}$ are generated by conducting the arc discharge method in a noble gas atmosphere [9–11]. A rather similar process is thought to have taken place before the formation of the Earth (or even the formation of the Solar System), leading to helium endofullerenes of extraterrestrial origin, encapsulated in ancient rocks [12].

Noble gas atom endofullerenes may also be synthesized by heating fullerenes under a high pressure of noble gas [9]. At high temperatures, orifices open temporarily in the fullerene cages, allowing admission of noble gas atoms, which are trapped when the cages reseal. Sometimes this leads to small quantities of fullerenes containing two atoms [13,14]. Such systems contain 'artificial molecules' of two, non-bonded noble gas atoms, constrained by the encapsulation to be very close in space [13–15].

It is also possible to implant atoms inside the fullerene cages by the use of accelerated ion beams. This produces small quantities of the remarkable single-atom endofullerenes $N@C_{60}$ and $P@C_{60}$ [16–18]. The atomic nitrogen endofullerene is also formed by a glow discharge method, which leads to a small amount of the molecular endofullerene $N_2@C_{60}$ as well [19].

These techniques only generate small amounts of molecular endofullerenes. An alternative approach, which uses relatively mild conditions, was demonstrated by Rubin *et al.* [20] and called 'molecular surgery'. This method consists of the following: (i) Controlled chemical reactions are carried out in which an orifice is opened in each fullerene cage through the addition of chemical moieties, usually followed by further reactions to widen the orifice to the size required for admission of the guest species. The result is an *open-cage fullerene*. (ii) A molecule or an atom is then introduced into the cavity, usually with the help of elevated temperature and pressure. This provides an *open-cage endofullerene*, which is often chemically stable under mild conditions, even though an orifice is available for the trapped molecule or atom to escape. (iii) A further series of chemical reactions is finally undertaken to close the orifice and to remove the additional chemical groups. An open-cage endofullerene containing a single dihydrogen (H_2) molecule was synthesized in this way, although the yield was limited [20].

A breakthrough was achieved by the group of Komatsu, who achieved a high-yield insertion of H_2 into an open-cage fullerene derivative [21], followed by complete reclosure of the orifice to obtain a chemically pure sample of $H_2@C_{60}$ [22]. Working on similar lines, the group of Murata [23] achieved the synthesis of the closed water endofullerene $H_2O@C_{60}$. These impressive synthetic feats have provided macroscopic quantities of small-molecule non-metallic endofullerenes for spectroscopic study. These achievements of synthetic chemistry underpin the science described in the rest of this review.

Isotopologues of $H_2@C_{60}$ and $H_2O@C_{60}$ such as $D_2@C_{60}$, $HD@C_{60}$, $HDO@C_{60}$ and $D_2O@C_{60}$ are now available through molecular surgery. The complete molecular surgical procedure with insertion of H_2 and reclosure of the cage has been achieved for C_{70} [24]. It is even possible to encapsulate two H_2 molecules inside the same closed C_{70} cage [24]. The partial encapsulation of larger molecules such as CO, NH_3 and CH_4 has been achieved in open-cage fullerenes with large orifices [25–27], although, at the time of writing, such cages have not yet been closed.

2. Molecular endofullerenes

Molecular endofullerenes may conveniently be divided into two classes: *metallic molecular endofullerenes*, in which the encapsulated molecule contains one or more metal atoms, and *non-metallic molecular endofullerenes* or *light-molecule endofullerenes*, which lack a metal atom.

Downloaded from rsta.royalsocietypublishing.org on August 12, 2013

The large subject of *metallic* endofullerenes is the subject of many other books and articles [2–4,6,7]. In most cases, the structure and behaviour of these species are discussed in terms of the preferred position and orientation of the endohedral species with respect to the cage. The large mass of the endohedral species justifies a classical approach.

The light-molecule endofullerenes discussed in this review consist of one or more molecules of low molecular mass encapsulated in closed or partially opened fullerene cages. The physical chemistry of light-molecule endofullerenes, in contrast to that of metallic endofullerenes, is dominated by the quantization of the encapsulated molecule. Since the mass and moment of inertia of the encapsulated molecule are small, and the confinement is tight, effects due to translational and rotational quantization are significant for small-molecule endofullerenes, even at room temperature. For example, in the seminal case of $H_2@C_{60}$, the spacing between the two lowest translational levels corresponds to about 260 K in temperature units, and the rotational energy level spacing is about 175 K [28–30]. Quantum effects are therefore considerable at room temperature and dominant even at moderately low temperatures. The trapped molecules cannot be considered as classical objects with well-defined position and orientation. The endohedral molecule is best imagined as a trapped 'molecular wave' that is confined to the endohedral region by the high barrier provided by the carbon skeleton. In this respect, the science of light-molecule endofullerenes is related to phenomena such as molecular quantum interference [31]. The behaviour of the trapped molecular wave is dominated by the nature of the trapping potential, and especially by its spatial symmetry.

(a) Cages

Figure 1 shows the structures of some of the fullerene cages used to encapsulate small non-metallic molecules.

(i) Closed fullerenes

At the time of writing, the fully closed forms of light-molecule endofullerenes have been obtained for C_{60} and C_{70}. The C_{60} cage has icosahedral symmetry (point group I_h). C_{70} has an elongated shape with point symmetry D_{5h}.

The natural isotopic distribution of carbon should be borne in mind. Although almost 99% of naturally occurring carbon atoms are ^{12}C (six protons and six neutrons in the nucleus, with nuclear spin zero), about 1.07% are ^{13}C, possessing an extra neutron. About 48% of C_{60} cages and about 53% of C_{70} cages contain at least one ^{13}C nucleus. The natural occurrence of ^{13}C nuclei in the fullerene cages allows the generation of nuclear magnetic resonance (NMR) signals from the cage, since ^{13}C has a nuclear spin quantum number of 1/2 and is weakly magnetic. Furthermore, the mass difference between ^{12}C and ^{13}C may be responsible for small perturbations in the shape of the cage and hence the symmetry of the endohedral potential, although such effects have not been observed unambiguously.

(ii) Open-cage fullerenes

The synthesis of closed endofullerenes by molecular surgery involves intermediates in which the molecule is encapsulated in a modified cage containing an orifice. The open-cage systems are interesting in their own right since the open cages often have low symmetry. In many cases, the open-cage forms lack any non-trivial symmetry element (point group C_1). Several examples are shown in figure 1. As discussed later, the asymmetric confining potential fully lifts the degeneracy of the confined molecular wave.

(iii) Exohedrally modified fullerenes

Chemical reactions may be conducted on fullerenes to attach chemical groups to the outside of the cage, but without opening it. A standard procedure is the Bingel reaction, which transforms one of the fullerene double bonds into an edge of a cyclopropane ring (figure 1*g* [33]). Another

Downloaded from rsta.royalsocietypublishing.org on August 12, 2013

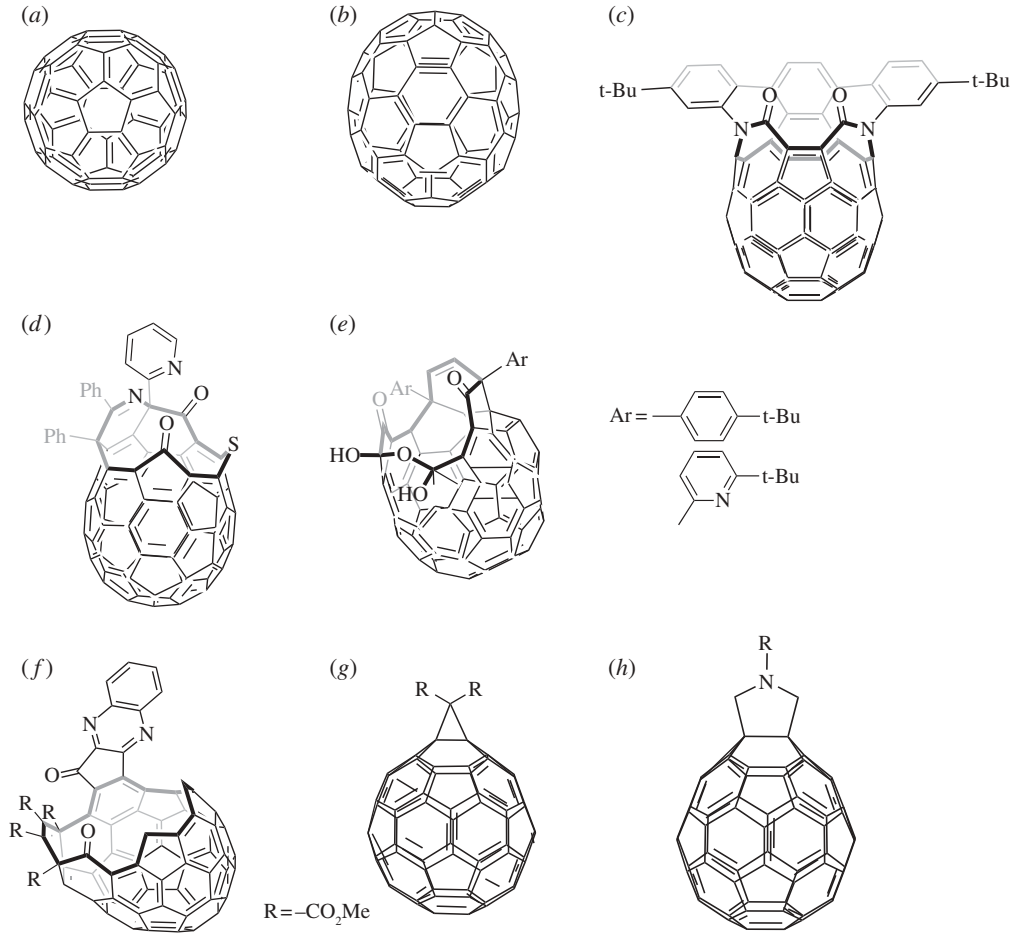

Figure 1. Fullerene cages used for encapsulating small molecules. (*a*) Closed C_{60} cage, (*b*) closed C_{70} cage, (*c*) open-cage form of Rubin *et al.* [20] used for encapsulating H_2, (*d*) open-cage form of Komatsu *et al.* [22] used for encapsulating H_2, (*e*) open-cage form of Kurotobi & Murata [23] used for encapsulating H_2O, (*f*) open-cage form of Iwamatsu *et al.* [32] used for encapsulating H_2O, (*g*) product of the Bingel [33] reaction on C_{60} and (*h*) product of the Prato reaction on C_{60} [34].

popular method is the Prato reaction, in which a five-membered pyrrolidine ring is formed (figure 1*h* [34]). The Prato method has been used to attach nitroxide-bearing side chains to endofullerenes, in order to investigate *ortho–para* conversion of endohedral H_2 induced by the nitroxide magnetism [35,36]. Apart from the direct influence of the attached groups on the endohedral molecules, exohedral modifications lower the cage symmetry, which influences the quantum energy level structure of the encapsulated molecule, as described later.

(iv) Fused-cage endofullerenes

The fullerene cages of $H_2@C_{60}$ have been fused by a mechanochemical method (high-speed vibration milling). This leads to a dumbell-shaped C_{120} molecule containing a H_2 molecule in each of two separate cavities [22].

(v) Fullerene anions

^{3}He endofullerenes have been reduced by chemical reactions, leading to species such as $^3He@C_{70}^{3-}$ and $^3He@C_{70}^{6-}$ [15,37]. At the time of writing, the only reported light-molecule endofullerene of this type is the 'artificial molecule' endofullerene $^3He_2@C_{70}^{6-}$ [15].

Downloaded from rsta.royalsocietypublishing.org on August 12, 2013

Table 1. Some light endohedral molecules and their properties.

molecule[a]	spin isomerism	electric dipole moment	rotational symmetry	cages	selected references
H_2	yes (fermion)	no	symmetric top	C_{60}, C_{70} and derivatives	[21,22,24,28–30,35,38–53]
HD	no	very weak	symmetric top	C_{60}, C_{70} and derivatives	[29,45,54,55]
D_2	yes (boson)	no	symmetric top	C_{60}, C_{70} and derivatives	[29,45,54,55]
$^{14}N_2$	yes (boson)	no	symmetric top	C_{60}	[19]
H_2O	yes (fermion)	yes	asymmetric top	C_{60} and derivatives	[23,32,56,57]
$^{3}He_2$*	yes (fermion)	no	symmetric top	C_{60}, C_{70} and derived anions	[13,15,37]
$^{20}Ne_2$*	yes (boson)	no	symmetric top	C_{70}	[14]
$2H_2$*	yes (boson)	no	symmetric top	C_{70} and derivatives	[24,58]
CO	no	yes	symmetric top	open-cage only	[25]
NH_3	yes (fermion)	yes	symmetric top	open-cage only	[27]
CH_4	yes (fermion)	no	spherical top	open-cage only	[26]

[a]'Artificial molecules' with no formal chemical bond, and generated by the confinement of two atoms or molecules in the same small cavity, are indicated by an asterisk.

(vi) Photo-excited triplet fullerenes

Illumination of fullerenes generates an excited electronic singlet state that decays to a relatively long-lived electronic triplet state, which displays electronic spin magnetism. Photo-excited triplet species such as $H_2@^3C_{60}$ and $H_2@^3C_{70}$ have been used for studies of photo-induced *ortho–para* conversion [38].

(b) Endohedral molecules

Table 1 summarizes some properties of the light endohedral molecules that have been encapsulated in fullerenes.

(i) Artificial molecules

Table 1 includes the 'artificial molecules' $^3He_2$ and Ne_2 that have been obtained in low yield by compressing two noble gas atoms into the same cavity [14,15]. In similar fashion, the two endohedral hydrogen molecules in $2H_2@C_{70}$ and its open-cage derivatives [24,58] form an artificial $(H_2)_2$ dimer.

(ii) Spin isomerism

One of the dominant features in the spectroscopy of molecular endofullerenes is the existence of nuclear spin isomers. This topic is discussed further in §3.

In order to exhibit spin isomerism, the molecule must have a symmetry element that exchanges two nuclei of exactly the same isotopic type. This is the case for dihydrogen H_2, where rotation by 180° perpendicular to the internuclear axis exchanges the two hydrogen nuclei. Spin isomerism also occurs for water, where a 180° rotation about the C_2 symmetry axis exchanges the two hydrogen nuclei.

As discussed in §3, the type of spin isomerism depends on whether the exchanged nuclei are fermions (half-odd-integer spin) or bosons (integer spin).

More complex forms of spin isomerism exist for the symmetrical polyatomic molecules NH_3 and CH_4 [59,60].

Spin isomerism is absent for asymmetric molecules such as HD and CO.

Downloaded from rsta.royalsocietypublishing.org on August 12, 2013

The 'artificial molecules' generated by confining two non-bonded noble gas atoms in the same cavity [14,15] are also expected to exhibit spin isomerism since the repulsive short-range interatomic forces require the atoms to 'chase each other around' in the small cavity, leading to the same spin-isomeric properties as an ordinary rotating molecule. The system $2H_2@C_{70}$ and its open-cage derivatives [24,58] display two levels of spin isomerism: each of the two endohedral molecules may be *ortho* or *para*, and in addition the *ortho–ortho* and *para–para* molecular pairs generate two-boson spin isomers.

(iii) Electric dipole moment

Interesting electrical properties have been postulated for endofullerenes in which the molecular guest possesses an electric dipole moment [61]. A solid crystal of such a substance comprises a regular array of freely rotating electric dipoles, which interact mutually through electrostatic forces. Cooperative phenomena such as ferroelectricity, in which electric dipoles align in a domain structure, are anticipated for such systems [61]. The water endofullerene $H_2O@C_{60}$ is a good candidate, but, at the time of writing, no experimental evidence of cooperative electric phenomena has been presented.

(iv) Rotational symmetry

In gas-phase rotational spectroscopy, molecules are conventionally classified using the (poorly named) categories of 'spherical tops' (molecules with tetrahedral symmetry or higher), 'symmetric tops' (molecules possessing at least one threefold or higher rotational axis) and 'asymmetric tops' (all others) [60]. Since molecules trapped in an endohedral potential experience an environment which resembles that of a molecular beam or a rarified gas, the same classification scheme proves to be relevant.

(c) Material phases

Molecular endofullerenes have been studied in solution and as solids.

(i) Isotropic solution

The primary tool for the characterization of molecular endofullerenes is solution NMR, as discussed later. A high-temperature liquid is a dynamic environment in which the fullerene cages rotate rapidly. All molecular orientations are equally probable in an ordinary isotropic liquid. Isotropic molecular tumbling leads to simplified NMR spectra, which are relatively easy to interpret.

(ii) Anisotropic solution

Atomic endofullerenes such as $N@C_{70}$ have been studied while dissolved in anisotropic liquids (liquid crystals). The elongated shape of the C_{70} molecule causes a partial orientation in the anisotropic phase, which splits the resonances of the electron paramagnetic resonance (EPR) spectrum of the endohedral atom [62]. Remarkably, the anisotropic splitting is also significant for $N@C_{60}$, where the cage is expected to have high symmetry [62]. This effect serves as a reminder that the fullerene cages are not rigid and may deform in response to the environment and also to the presence of endohedral species.

At the time of writing, there have been no reports of endohedral molecular fullerenes studied in anisotropic solution.

(iii) Solids

Experiments involving the quantization of the endohedral molecular species are usually conducted at low temperature, where the substances are solids.

Downloaded from rsta.royalsocietypublishing.org on August 12, 2013

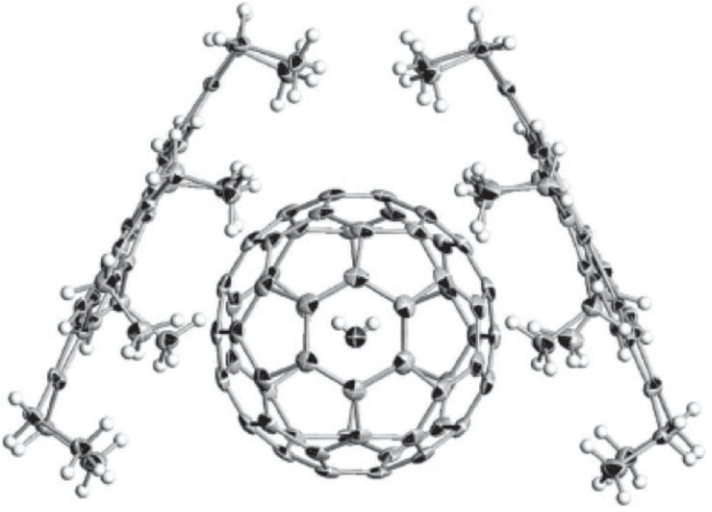

Figure 2. X-ray crystal structure of the molecular complex $H_2O@C_{60}\cdot(NiOEP)_2$, where NiOEP is nickel(II) octaethylporphyrin, showing the H_2O molecule inside the fullerene cage. Adapted from Kurotobi & Murata [23].

The properties of fullerenes in the solid state have been studied intensively. A range of solid-state phases are known, involving different modes of molecular organization in the crystalline state, and a variety of molecular motional effects [63]. For example, at ambient pressure, pure C_{60} forms a face-centred cubic phase above approximately 261 K, in which the C_{60} molecules rotate rapidly and isotropically. A simple cubic phase is formed below approximately 261 K in which the molecules rotate around threefold axes and in which correlations develop between the orientations of neighbouring C_{60} molecules [63]. Solid-state NMR data show that large-amplitude rotational jumps occur in this phase at temperatures down to approximately 100 K [64].

The phase behaviour of solid C_{70} is more complex, with at least five solid phases exhibiting different degrees of molecular rotation and intermolecular organization [63]. The molecular motion in the phases of solid C_{70} has been studied by solid-state NMR [65]. NMR spectroscopy of the endofullerene $H_2@C_{70}$ indicates that the long axes of the C_{70} cages orient along an applied magnetic field, at low temperature [53].

The material phase behaviour of open-cage and exohedrally modified fullerenes is presumably much simpler, since the reduced molecular symmetry strongly inhibits large-angle rotational motion of the molecular cages.

At the time of writing, the solid-state phase behaviour of endohedral molecular fullerenes is not known in detail. The fact that endohedral species do influence intermolecular forces is evidenced by the separation of endohedral and empty fullerenes by chromatography. ^{13}C solid-state NMR of $H_2@C_{60}$ shows a strong similarity to that of C_{60}, suggesting that the material phases are very similar [39].

One should bear in mind that many of the solid samples studied to date are not highly pure and crystalline. For example, it is known that many solid samples contain occluded solvent molecules, such as toluene or CS_2, as a by-product of the purification process. In addition, some samples contain a significant fraction of unoccupied cages. Improvements in synthetic and purification technologies are now leading to purer and more crystalline solid-state preparations, which could have a positive impact on the quality and interpretation of future spectroscopic results.

A well-ordered solid-state environment allows the use of X-ray crystallography to study the organization of the fullerene cages and to visualize the encapsulated molecules. An X-ray structure of a pure $H_2@C_{60}$ sample has been obtained by powder diffraction, showing the presence of the hydrogen molecule inside the cage [40]. Figure 2 shows a single-crystal X-ray structure of the endofullerene $H_2O@C_{60}$ co-crystallized with a nickel porphyrin [23].

Downloaded from rsta.royalsocietypublishing.org on August 12, 2013

3. Quantization

The spectroscopy of endohedral molecular fullerenes requires consideration of the quantum energy level structure and eigenstates of the endohedral molecular systems. The problem is conveniently discussed in four stages: (i) the quantization of the molecular degrees of freedom in the absence of the cage, (ii) quantization associated with the molecular confinement, (iii) the interaction between molecular quantization and confinement quantization, and (iv) the effect of reduced cage symmetry.

This brief summary will avoid mathematical formalism. Detailed theory, including the explicit Hamiltonians and energy expressions, is provided by Mamone [41].

(a) Internal molecular quantization

The quantum energy levels of the endohedral molecules may be discussed using the traditional categories of molecular spectroscopy—arranged in order of decreasing energy, these are electronic energy, vibrational energy, rotational energy and nuclear magnetic energy.

(i) Electronic quantization

Since the visible/ultraviolet spectroscopies are not considered here, and all of the molecules studied so far have singlet electronic ground states, the electronic modes are not of direct interest.

(ii) Vibrational quantization

Vibrational degrees of freedom are excited in mid-infrared (MIR) spectroscopy. This technique has been applied to $H_2@C_{60}$ [30,42,43], HD@C60 [66] and $D_2@C60$ [66]. Encapsulation in the cage gives a small red shift to the vibrational frequency of H_2 [30,42] and endows infrared activity to the vibrational modes of H_2, which are normally infrared-silent [41–43]. This phenomenon is known for H_2 trapped in other confined environments [67–69].

(iii) Rotational quantization: diatomics

For diatomic molecules such as H_2, the rotational energy levels are given in the rigid-rotor approximation by

$$E_J = BJ(J+1). \tag{3.1}$$

Here B is the rotational constant, given by $B = \hbar^2/2\mu_I$, where μ_I is the molecular inertial moment (the conventional symbol I is avoided here, owing to a conflict with notation for the nuclear spin); J is the rotational quantum number, $J \in \{0, 1, 2, \ldots\}$. The rotational degeneracies are given by $g_J = 2J + 1$, corresponding to the values of the magnetic quantum number for each rotational state, $M_J \in \{-J, -J+1, \ldots, +J\}$. The splitting between the lowest two rotational levels ($J = 0$ and $J = 1$) is equal to $2B$. In the case of H_2, the rotational splitting in wavenumbers is given by $2B/hc = 121.6\,\mathrm{cm}^{-1}$, which corresponds to a temperature of $2B/k_\mathrm{B} = 175.0\,\mathrm{K}$, where k_B is the Boltzmann constant. In the case of D_2, the relevant energies are $2B/hc = 60.9\,\mathrm{cm}^{-1}$ and $2B/k_\mathrm{B} = 87.6\,\mathrm{K}$. As noted earlier, these are significant energies, even relative to room temperature.

The rotational states $|J, M_J\rangle$ of a diatomic molecule are proportional to spherical harmonics, and have the spatial symmetry of atomic orbitals. The state $|0, 0\rangle$ is spherically symmetric, like an s-orbital, while the $J = 1$ states $|1, -1\rangle$, $|1, 0\rangle$, $|1, +1\rangle$ have the symmetry of p-orbitals. The five $J = 2$, states $|2, -2\rangle$, $|2, -1\rangle$, $|2, 0\rangle$, $|2, +1\rangle$ and $|2, +2\rangle$ have the symmetry of d-orbitals, and so on. Since the ground state $|0, 0\rangle$ is spherically symmetric, a molecule in an unperturbed $J = 0$ state cannot possess an electric dipole moment [70]. This applies even to heteroatomic diatomics such as HCl.

In the case of homonuclear diatomics, rotation of the molecule through 180° exchanges the positions of identical nuclei. The spin-statistics theorem of Fierz [71] and Pauli [72] requires that the total quantum state is antisymmetric with respect to the exchange of two fermions,

Downloaded from rsta.royalsocietypublishing.org on August 12, 2013

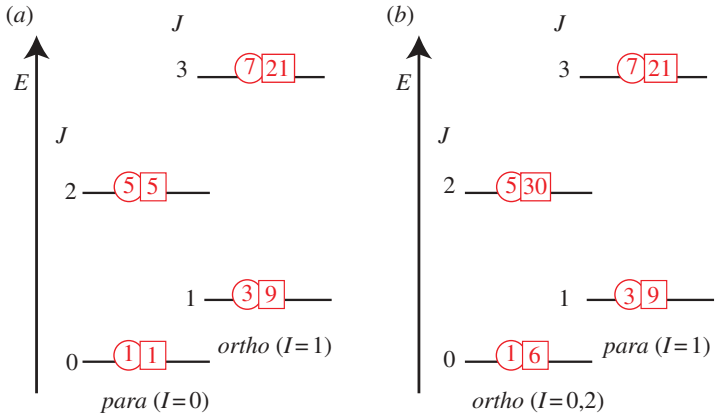

Figure 3. Rotational energy levels of (*a*) H_2 and (*b*) D_2, showing the *ortho–para* spin isomers. Spatial degeneracy is shown by numbers in circles. Total degeneracy, including nuclear spin degeneracy, is shown by numbers in squares. Fine structure caused by spin–rotation, dipole–dipole, quadrupolar and Zeeman couplings is ignored. The vertical scales are not the same in (*a*) and (*b*): in reality, the energy levels of D_2 are more closely spaced than those of H_2. (Online version in colour.)

and symmetric with respect to the exchange of two bosons. As predicted by Heisenberg, and cited in his 1932 Nobel Prize award, this principle entangles the rotational states of diatomic molecules with nuclear spin states, and leads to the incidence of nuclear spin isomers, with different symmetries for the nuclear spin states and rotational levels. In the case of H_2, where the atomic nuclei (protons) are fermions (nuclear spin $= 1/2$), the spin isomers are called *parahydrogen* (even-numbered rotational states and total nuclear spin $= 0$) and *orthohydrogen* (odd-numbered rotational states and total nuclear spin $= 1$) [73]. In the case of D_2, where the atomic nuclei are bosons (nuclear spin $= 1$), the spin isomers are called *paradeuterium* (odd-numbered rotational states and total nuclear spin $= 1$) and *orthodeuterium* (even-numbered rotational states and total nuclear spin $= 0$ or 2) [73]. In most circumstances, exchange of the spin isomers is slow, since a change in the rotational quantum number (which is usually readily accomplished by collisions) must be accompanied by an *asymmetric* change in the nuclear spin states for spin isomerization to occur (i.e. the two nuclei must experience different local interactions). In the case of hydrogen, spin-isomer conversion is particularly slow, since protons (which have spin $= 1/2$) have a spherical electric charge distribution, so that a change in total nuclear spin state requires a coupling to magnetic fields that are inhomogeneous on a molecular distance scale. In the case of deuterium, the electric quadrupole moment of the spin $= 1$ deuterium nuclei allows a coupling to local electric field gradients, which provides a non-magnetic mechanism for *ortho–para* conversion [74].

An important consequence of slow spin-isomer conversion is the persistence of metastable *ortho*-species (for H_2) and *para*-species (for D_2), even at temperatures much lower than the $J = 0$ to $J = 1$ splitting.

The Pauli principle does not apply to heteronuclear diatomics such as HD. As a result, HD does not have spin isomers, and molecules cannot be trapped in metastable states with $J \neq 0$.

The lowest rotational energy levels and spin isomers of homonuclear diatomics are summarized in figure 3. This diagram shows the degeneracies of the spatial states (ignoring fine structure) and the total degeneracies including the nuclear spins. The total degeneracies of these levels can be remarkably high: for example, the $J = 2$ level of orthodeuterium has a 30-fold degeneracy.

(iv) Rotational quantization: polyatomics

The rotational energy level structure of larger molecules such as H_2O is more complex since there is an additional degree of rotational freedom. A good modern exposition of the rotational

Downloaded from rsta.royalsocietypublishing.org on August 12, 2013

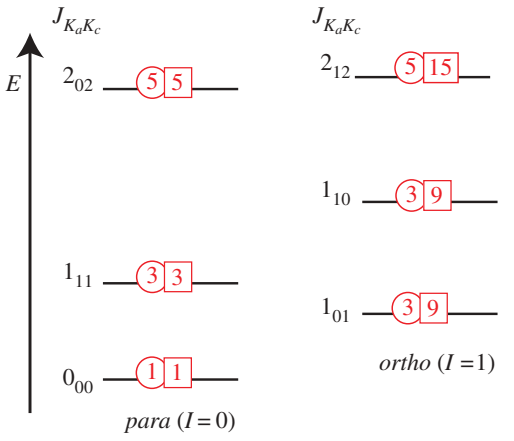

Figure 4. The lowest rotational energy levels of H_2O. Spatial degeneracy is shown by numbers in circles. Total degeneracy, including nuclear spin degeneracy, is shown by numbers in squares. Fine structure caused by spin–rotation, dipole–dipole, quadrupolar and Zeeman couplings is ignored. (Online version in colour.)

energy levels, eigenstates, degeneracies and spin isomerism of polyatomic molecules is given by Bunker & Jensen [60]. The rotational states of an asymmetric top such as H_2O are conventionally labelled as $J_{K_aK_c}$, where the rotational quantum number takes values $J \in \{0, 1, 2, \ldots\}$, as in the diatomic case. The subscripts K_a and K_c are technically not quantum numbers, but indicate the correspondence of the asymmetric top rotational state with the related states of a symmetric top [60]. Bunker & Jensen [60] propose a more informative notation that indicates the symmetry of the molecular wave function; for convenience, we stick with the historical notation. For each rotational state with quantum number J, there are $2J + 1$ possible combinations of labels K_a and K_c. Furthermore, each level $J_{K_aK_c}$ is $(2J + 1)$-fold degenerate, with the magnetic quantum number taking values $M_J \in \{-J, -J + 1, \ldots, +J\}$.

The Pauli principle entangles the rotational and nuclear spin states of symmetrical molecules such as H_2O, leading to the formation of spin isomers. In the ground vibrational state, *para*-water states have total nuclear spin $I = 0$, and even values of $K_a + K_c$, while ortho-water states have total nuclear spin $I = 1$ and odd values of $K_a + K_c$. As in the case of diatomics, spin-isomer conversion can be slow. The physical separation of liquid *ortho*- and *para*-water has been described [75], although the claim is disputed.

The ground rotational state 0_{00} of *para*-water is spherically symmetric and does not have an electric dipole moment. It is hard to visualize a spherical water molecule, but quantum mechanics is unequivocal about its existence.

The lowest rotational energy levels and spin isomers of H_2O are summarized in figure 4.

(v) Magnetic quantization

Although NMR spectroscopists are familiar with the magnetic moments of nuclei with spin > 0, and their Zeeman splitting in a magnetic field, many are surprised to learn that *rotational* states of molecules with $J > 0$ are also associated with magnetic moments, and display Zeeman splittings in a magnetic field. Phenomena such as precession and nutation in a magnetic field, which are central topics in NMR [76,77], are also observed for the *rotational* angular momenta of molecules. For example, the *molecular* magnetic resonance of $J = 1$ *ortho*-H_2 is observed at approximately one-sixth of the proton Larmor frequency, in the same magnetic field [78,79].

Nuclear spin angular momenta and molecular rotational angular momenta may couple, in much the same way as two nuclear spins in the same molecule. Consider, for example, the *ortho*-H_2 ground state, which has molecular angular momentum $J = 1$ and nuclear spin angular momentum $I = 1$. The magnetic resonance spectrum at the proton Larmor frequency displays *six*

Downloaded from rsta.royalsocietypublishing.org on August 12, 2013

peaks, since the two single-quantum transitions of the $I = 1$ nuclear spin are both split into three components by coupling to the $J = 1$ molecular angular momentum [78,79]. A similar spectrum is obtained at the molecular resonance frequency, in this case because the two single-quantum transitions of the $J = 1$ 'molecular spin' are split into three components by coupling to the $I = 1$ nuclear angular momentum [78,79]. These phenomena were observed and described with great detail and clarity by Ramsey and co-workers [78,80,81] well before the bulk NMR experiments of Purcell, Pound and Bloch.

These phenomena are unfamiliar to most magnetic resonance spectroscopists, because they are only observed in rarified *molecular beams*, in which intermolecular collisions are infrequent. They are not observed in ordinary gases or liquids, since collisions cause rapid rotational transitions, which average to zero the splitting structure caused by coupling to the molecular angular momentum. For example, the NMR spectrum of H_2 in the gas phase, or in isotropic solution, is a single peak, with no obvious evidence of coupling between the nuclei and the molecular angular momenta. Similarly, in solids, the rotational angular momentum is quenched by local fields.

Although the coupling between spin and molecular angular momenta leads to no obvious spectral effects in bulk NMR, modulation of this coupling by molecular collisions does provide an important relaxation mechanism for nuclear spins, especially in gases. This is the *spin–rotation* relaxation mechanism [76,82].

The highly symmetrical and protected environment of a fullerene cavity resembles, to some extent, that of a molecular beam. The possibility arises of observing, in bulk matter, spectral structure associated with coherent coupling between the nuclear and molecular angular momenta of endofullerene guest molecules. However, at the time of writing, no such structure has been observed.

(b) Translational quantization

A molecule trapped inside a fullerene cavity experiences translational quantization. The translational molecular wave functions are solutions of the time-independent Schrödinger equation in the confining potential.

Hartree–Fock quantum calculations of H_2 inside C_{60} showed that the potential function has a minimum at the centre of the cage, with an approximately quadratic dependence on displacement from the centre [44]. The translational potential of H_2 inside C_{60} is therefore close to that of an ideal three-dimensional harmonic oscillator, but with a small additional quartic potential term, and a weak dependence on the orientation of the H_2 molecule with respect to the cavity wall [44]. Unlike some metallo-fullerenes, there is no potential minimum for the H_2 molecule near the internal wall of the cavity, and there is no potential barrier for the rotation of the H_2 molecule.

Similar results for the potential are obtained by summing empirical Lennard-Jones potential terms for the interaction of the endohedral molecule with each carbon atom of the cage [45–47]. In the case of C_{70}, the confining potential for H_2 displays two very weak minima displaced from each other along the long axis of the elongated cage [47]. These minima are too shallow to localize the H_2 molecules.

The Schrödinger equation may be solved to obtain the translational eigenstates and energies of the molecule inside the cavity. As an initial approximation, the internal molecular degrees of freedom may be ignored. Some highly simplified potential models may be solved analytically: for example, a particle confined to the interior of a three-dimensional sphere has straightforward analytical solutions [28]. A better approximation is offered by a three-dimensional harmonic oscillator, which may also be solved analytically (figure 5 [83]). In the case of an isotropic harmonic oscillator (equal force constants in all three directions, such as for $H_2@C_{60}$), the energy level structure and quantum wave functions resemble those of the hydrogen atom. There is a principal quantum number n, which takes values $n \in \{0, 1, 2, \ldots\}$, and which determines the energy through $E_n = \hbar\omega_{\mathrm{tr}}(n + 3/2)$. Here, ω_{tr} is the translational oscillation frequency, given by $\omega_{\mathrm{tr}} = (k_{\mathrm{F}}/m_{\mathrm{mol}})^{1/2}$, where m_{mol} is the mass of the endohedral molecule and k_{F} is the potential force constant. The orbital angular momentum quantum number ℓ, representing the circulatory motion of the

Downloaded from rsta.royalsocietypublishing.org on August 12, 2013

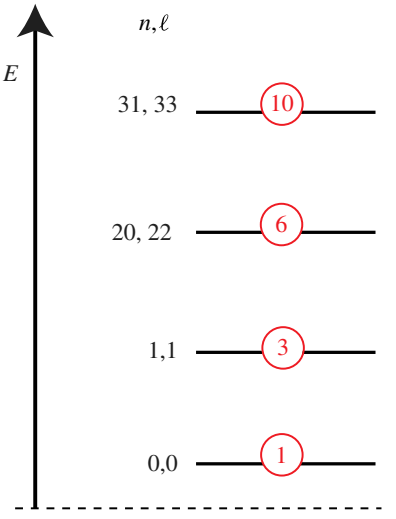

Figure 5. Lowest energy levels of an isotropic three-dimensional harmonic oscillator. The spatial degeneracies are shown by numbers in circles. The offset of the lowest level from the minimum of the potential well (dashed line) is the zero-point energy. (Online version in colour.)

molecule inside the cavity, takes values $\ell \in \{0, 2, \ldots, n\}$ for n even and $\ell \in \{1, 3, \ldots, n\}$ for n odd, but has no effect on the energy (just as for the H atom). Each $|n, \ell\rangle$ state is $(2\ell + 1)$-fold degenerate, with the magnetic quantum number m_ℓ taking values $m_\ell \in \{-\ell, -\ell + 1, \ldots, +\ell\}$. The zero-point energy of the three-dimensional harmonic oscillator is $E_0 = (3/2)\hbar\omega_{\mathrm{tr}}$. The total degeneracy of the energy level with principal quantum number n is $g_n = (n + 1)(n + 2)/2$ (contrast the case of the H atom, where the degeneracy is $g_n = n^2$). The lowest levels of the isotropic three-dimensional harmonic oscillator are sketched in figure 5.

The translational energy level splittings are large for small-molecule endofullerenes. The translational frequency for H_2 inside C_{60} is $\omega_{\mathrm{tr}}/2\pi c \sim 180\,\mathrm{cm}^{-1}$, which is in the far-infrared (FIR) region of the electromagnetic spectrum (wavelength $2\pi c/\omega_{\mathrm{tr}} \sim 55\,\mu\mathrm{m}$). This translational energy corresponds to a temperature of $\hbar\omega_{\mathrm{tr}}/k_{\mathrm{B}} \sim 260\,\mathrm{K}$, indicating that translational quantization is very much present even at room temperature. For these systems, the translational splittings are even larger than the rotational splittings.

At low temperature ($T \lesssim 100\,\mathrm{K}$), systems such as $H_2@C_{60}$ may therefore be assumed to occupy the translational ground state, with a molecular wave function given by a Gaussian shape centred at the centre of the cavity and with no orbital angular momentum.

More massive endohedral molecules such as H_2O have smaller translational splittings. In that case, excited translational levels are populated at relatively low temperature.

(c) Translation–rotation coupling

Endohedral molecules have both rotational and translational degrees of freedom. Since the confining potential depends on molecular orientation with respect to the cage, the translational and rotational modes are coupled.

This problem is tackled by introducing a quantum number λ for the coupled rotational and orbital angular momentum [41,43,45,46,84]. The coupled angular momentum quantum number takes values obeying the triangle rule: $\lambda \in \{|\ell - J|, |\ell - J| + 1, \ldots, |\ell + J|\}$. For example, a state with $\{\ell, J\} = \{0, 0\}$ can only have $\lambda = 0$, indicating no orbital or rotational motion. If the quantum numbers are $\{\ell, J, \lambda\} = \{1, 0, 1\}$, then the coupled angular momentum $\lambda = 1$ is purely orbital; whereas if the quantum numbers are $\{\ell, J, \lambda\} = \{0, 1, 1\}$, then the coupled angular momentum $\lambda = 1$ is purely rotational. The quantum numbers $\{\ell, J, \lambda\} = \{1, 1, 0\}$ indicate orbital

Downloaded from rsta.royalsocietypublishing.org on August 12, 2013

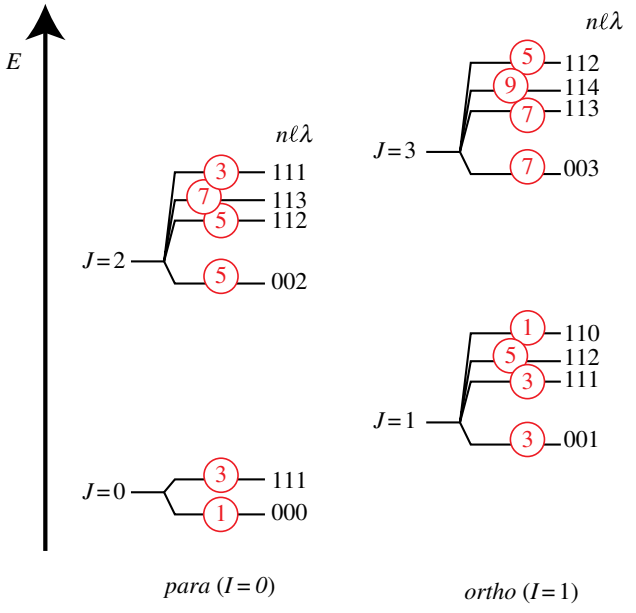

Figure 6. Coupled translation–rotation energy level scheme for a homonuclear diatomic molecule with fermion nuclei, in a spherical potential. The spatial degeneracies of the sublevels are shown by circled numbers. The spin degeneracies are 1 for the *para* states and 3 for the *ortho* states. The vertical energy scale is not accurate. (Online version in colour.)

and rotational motions in the opposite sense, so that the total angular momentum cancels out. The quantum numbers $\{\ell, J, \lambda\} = \{1, 1, 2\}$ indicate orbital and rotational motions in the same sense, and adding up.

In a spherical environment, a level with quantum number λ is $(2\lambda + 1)$-fold degenerate, with the magnetic quantum number taking values $m_\lambda \in \{-\lambda, -\lambda + 1, \ldots, +\lambda\}$.

For a diatomic molecule, the potential energy function is five-dimensional (three dimensions for the position of the molecule in the cavity, and two to represent the spatial orientation of the molecule). In the case of $H_2@C_{60}$, the terms in the five-dimensional potential, including translation–rotation couplings, have been estimated by fitting experimental infrared absorption frequencies [30,41,43]. The five-dimensional potential is calculated by summing Lennard-Jones pairwise potentials between the endohedral molecule and all carbon atoms. The molecular eigenfunctions and energies are obtained by numerical solution of the five-dimensional Schrödinger equation [45–47]. A good match between the experimental infrared data and the computed quantum levels was achieved by representing the potential between H_2 and each carbon atom as a sum of *three* Lennard-Jones terms, one of which involves the interaction of the carbon atom with a virtual atom at the centre of the H_2 molecule [47]. The relative weights and coefficients of the three Lennard-Jones terms are adjusted to obtain a good fit to the experimental data.

A coupled translation–rotation energy level scheme for $H_2@C_{60}$ is shown in figure 6. Note the irregular ordering of the λ sublevels.

(d) Reduced symmetry

Strictly speaking, the discussion above concerns idealized cages with perfect spherical symmetry. In practice, even C_{60} provides an icosahedral potential, not a spherical one. Often, the symmetry of the encapsulating cage is reduced further. This may be due to modifications of the cage structure (for example, C_{70}), the isotopic distribution of ^{13}C, the opening of a cavity in the cage, exohedral modifications of the cage or external influences such as solid-state crystal fields or

Downloaded from rsta.royalsocietypublishing.org on August 12, 2013

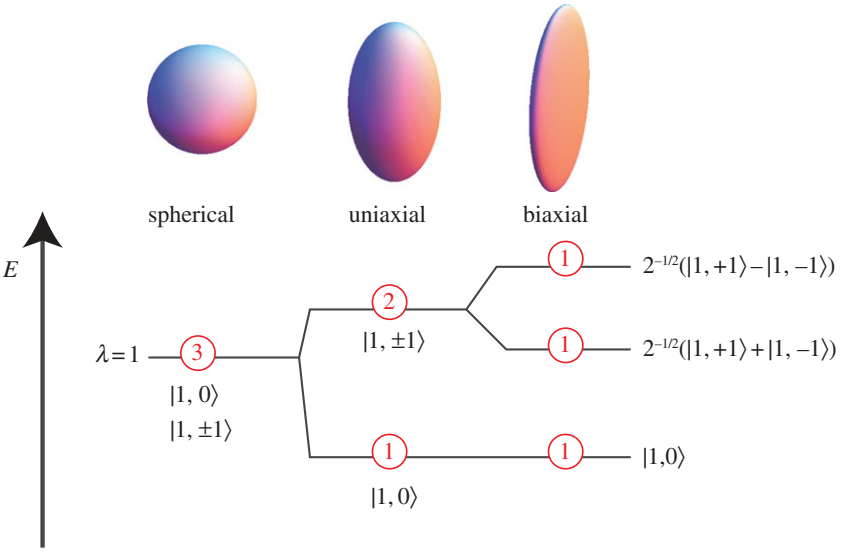

Figure 7. Breaking of degeneracy by reduction of the cage symmetry, for a $\lambda = 1$ translation–rotation state. The state is threefold degenerate in a spherically symmetric (or icosahedral) potential. A uniaxial perturbation of the potential partially lifts the degeneracy. If the uniaxial perturbation is small, there is negligible mixing between states with different values of λ, but the states with different values of $|m_\lambda|$ have different energies. If the potential has a small biaxial perturbation, the spatial degeneracy is completely lifted and the spatial eigenstates consist of the state with $m_\lambda = 0$ and the symmetric and antisymmetric combinations of the states with $m_\lambda = \pm 1$. Each of these three states has zero angular momentum along one of the principal axes of the biaxial potential. (Online version in colour.)

the anisotropic environment of a liquid crystal solvent. In some cases, such as $H_2O@C_{60}$, there is experimental evidence for a reduction in symmetry, but the origin is unknown at the present time [56].

In general, a reduction in symmetry lifts the degeneracy of the rotational–translational states, and mixes states with different values of the quantum numbers λ or m_λ (figure 7).

(i) Icosahedral symmetry

Icosahedral symmetry provides vanishing matrix elements for all spherical tensors of odd ranks, and also all even ranks between 2 and 14, inclusive, with the exception of ranks 6, 10 and 12 [85]. The practical consequences of this are that, in general, the spherical eigenfunctions with total angular momentum λ are not exact eigenfunctions of the cage potential and are mixed with other eigenfunctions with angular momentum $\lambda \pm 6$, $\lambda \pm 10$ and $\lambda \pm 12$. However, the mixing coefficients are usually small, so that, for rotation–translation states of low angular momentum, the consequences are minor. It is normally a good approximation to treat an undistorted C_{60} cage as being spherical.

(ii) Uniaxial distortion

In many cases, the icosahedral symmetry of C_{60} is broken by a perturbation in one direction, with the perpendicular directions remaining equivalent. This is the case in C_{70} and is likely to apply to several exohedral modifications of C_{60} and possibly in $H_2O@C_{60}$ as well.

The first-order effect of a uniaxial distortion is to partially lift the degeneracy of the translation–rotation states. In general, a $(2\lambda + 1)$-fold degenerate state with total angular momentum λ is split into $\lambda + 1$ levels, with quantum numbers $m_\lambda \in \{0, \pm 1, \pm 2, \ldots, \pm\lambda\}$. These states have angular momenta $m_\lambda \hbar$ along the unique axis of the cage. To first order, the corresponding spatial eigenfunctions are the same as the spherical eigenfunctions, i.e. $|\lambda, m_\lambda\rangle$ but with a quantization axis defined by the cage distortion. To second and higher order in the perturbation, eigenfunctions

Downloaded from rsta.royalsocietypublishing.org on August 12, 2013

$|\lambda, m_\lambda\rangle$ may be mixed with eigenfunctions $|\lambda \pm 2, m_\lambda\rangle$, $|\lambda \pm 4, m_\lambda\rangle$, etc. For example, the isotropic spherical ground state $|0,0\rangle$ may be mixed with the states $|2,0\rangle$, $|4,0\rangle$, etc., perturbing its pure spherical symmetry. Note, however, that the quantum number m_λ is always conserved for a perturbation with full uniaxial symmetry. Numerical computations of the translation–rotation energy level structure have been completed for $H_2@C_{70}$ and show the expected degeneracy pattern [47,53].

(iii) Biaxial or asymmetric distortion

An arbitrary distortion of the cage breaks the symmetry completely. This is usually the case for the open-cage variants. The first-order effect of an asymmetric perturbation is to completely lift the degeneracy of the level with total angular momentum λ, generating $2\lambda + 1$ non-degenerate states with different energy. For example, a level with total angular momentum $\lambda = 1$ splits into three levels. In general, the quantum number m_λ is no longer a good quantum number for the perturbed states. In the case of a small biaxial perturbation applied to a $\lambda = 1$ state, the three perturbed states have the form $|1,0\rangle$, $2^{-1/2}(|1,+1\rangle + |1,-1\rangle)$ and $2^{-1/2}(|1,+1\rangle - |1,-1\rangle)$. These eigenfunctions correspond to states with zero angular momentum along three orthogonal axes (the principal axes of the perturbing quadratic potential). This phenomenon corresponds to the quenching of angular momentum by an asymmetric perturbation.

Large asymmetric perturbations mix together states with many different values of λ and m_λ, and it becomes difficult to make general statements.

The effect of small symmetry-breaking perturbation on a $\lambda = 1$ level is summarized in figure 7.

4. Spectroscopy of molecular endofullerenes

Spectroscopic studies of molecular endofullerenes may be conducted using photons (electromagnetic spectroscopy) or by massive particles such as neutrons. The main forms of electromagnetic spectroscopy are classified according to photon energy. In order of increasing energy, these are: radiofrequency spectroscopy (in particular, NMR), microwave and FIR spectroscopy, MIR spectroscopy, visible and ultraviolet spectroscopy and X-ray spectroscopy. In addition, there are inelastic scattering spectroscopies such as inelastic neutron scattering (INS) and inelastic photon scattering (Raman spectroscopy).

In broad terms, the high-energy spectroscopies provide information on the cages, while infrared spectroscopy and neutron scattering allow study of the rotational–translational energy levels of the endohedral molecules. NMR provides a more detailed insight into the ordering, dynamics and spatial eigenfunctions of the encapsulated molecules, and also the symmetry and dynamics of the encapsulating cages.

(a) Ultraviolet and visible spectroscopy

At the time of writing, visible and ultraviolet (UV/vis) spectroscopies are uninformative for small-molecule endofullerenes, since the host molecules are not chromophores in the UV/vis spectral region, and the strong broad absorption bands of the fullerene cage are almost unaffected by the presence of the light endohedral molecules, at least in the case of $H_2@C_{60}$ [22] and $H_2O@C_{60}$ [23].

Pump–probe pulsed laser spectroscopy has been used for the measurement of photo-excited triplet lifetimes in $H_2@C_{60}$ and $H_2@C_{70}$ [38].

Attempts at Raman spectroscopy have been made, but the weak inelastic light scattering is masked by the strong fluorescence of the fullerene cages [86].

(b) Infrared spectroscopy

Infrared spectroscopy is a particularly informative method for characterizing the quantized rotation–translation levels of endohedral small molecules, and for tracking the progress of spin-isomer conversion.

Downloaded from rsta.royalsocietypublishing.org on August 12, 2013

(i) Mid-infrared spectroscopy

MIR spectroscopy (in the rough wavelength range 2–25 μm or 400–5000 cm^{-1} in wavenumbers) has been used to detect transitions from the $v = 0$ vibrational ground state to the $v = 1$ vibrational excited state of endohedral H_2 [30,42]. The vibrational excitation is accompanied by simultaneous translational and rotational excitations, leading to a rich fine structure, from which energy level spacings may be elucidated in the vibrational excited state. The homogeneous and symmetrical environment of the H_2 molecules in the endofullerenes leads to well-resolved vibrational structure, which may be interpreted quantitatively [30,42,43,66].

When such experiments are conducted on samples at around 4 K, infrared absorption occurs starting from molecules with no translational or rotational excitation. The spectral structure is therefore generated by the sublevel structure of the vibrational excited state. At higher temperature, infrared absorption lines are also observed starting from excited rotational–translational sublevels of the vibrational ground state. This allows estimation of the energy level structure in the vibrational ground state, as well as that of the vibrational excited state [30].

Infrared absorption by homonuclear diatomics such as H_2 does not occur in low-pressure gases since the molecule has no permanent dipole moment, and the only vibrational mode is symmetric. Nevertheless, weak vibrational transitions are induced by infrared radiation in the case that the diatomic molecule experiences an asymmetric environment—even transiently. This occurs in pressurized gases during intermolecular collisions [87] or for molecules trapped inside cavities [69,88–90]. In the case of molecular endofullerenes, the infrared-active vibrational transitions are a subset of all possible transitions, governed by selection rules for the changes in n, ℓ and λ quantum numbers [41,42]. Since the electromagnetic field does not induce a change in the nuclear spin quantum number, infrared transitions only occur between states of the same spin isomer, i.e. *ortho*-to-*ortho* and *para*-to-*para*, but not *ortho*-to-*para* or *para*-to-*ortho*.

MIR absorption peaks of $H_2@C_{60}$ are compared with numerical simulations using a fitted model of the endohedral potential in figure 8. The match between experiment and simulation is good, although some experimental peaks display small splittings that do not appear in the simulated spectra. The origin of these splittings is not yet known, but they could be due to environment-induced cage distortions, sample inhomogeneity or the presence of ^{13}C fullerene isotopologues.

(ii) Far-infrared spectroscopy

In suitable cases, FIR spectroscopy (in the rough wavelength range 25 μm to 1 mm or 10–400 cm^{-1} in wavenumbers) may be used to detect rotation–vibration transitions, without accompanying vibrational excitation [56]. The conversion of *ortho*-water to *para*-water in $H_2O@C_{60}$ has been monitored through a slow change in the relative intensities of the *ortho* and *para* FIR peaks [56].

(c) Inelastic neutron scattering

INS is a very powerful technique for studying the quantized energy levels and the spatial distribution of molecular wave functions. The main disadvantage of INS is that relatively large amounts of sample (tens to hundreds of milligrams of endohedral fullerenes) are necessary to obtain an informative spectrum. The existence of INS data on small-molecule endofullerenes [29,43,48,49] is due to the development of the high-yield synthetic methods described earlier and heroic efforts by several synthetic research teams.

A monochromatic neutron beam may either pick up energy from a molecular system upon scattering (neutron energy gain) or deposit part of its energy in the system (neutron energy loss). Measurement of the scattering intensity as a function of the change in neutron energy provides an INS spectrum. By convention, the energy change is specified for the system under study (not the neutron beam), so that neutron energy *gain* corresponds to *negative* values of ΔE, while

Downloaded from rsta.royalsocietypublishing.org on August 12, 2013

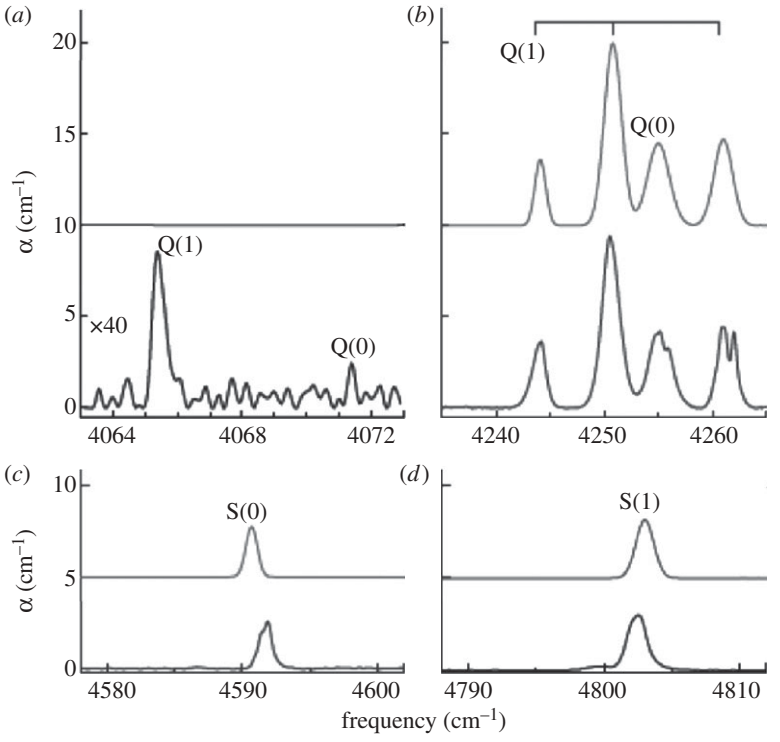

Figure 8. MIR absorption peaks of $H_2@C_{60}$ at a temperature of 6 K. In each infrared region, the lower curve shows the experimental spectrum, whereas the upper curve shows a simulation using a best-fitting model for the translation–rotation potential. Reprinted with permission from Mamone *et al.* [42]. Copyright 2009, American Institute of Physics.

neutron energy *loss* corresponds to *positive* values of ΔE. An INS spectrum for $H_2@C_{60}$ at low temperature (1.6 K) is shown in figure 9. The neutron energy gain and loss branches are on the left and right, respectively.

The INS spectra of systems displaying spin isomerism include transitions between different spin isomers. These transitions are unobserved in electromagnetic spectroscopies, since the wavelength of ordinary electromagnetic radiation is long compared with molecular dimensions, leading to strong conservation of the total nuclear spin quantum number. Neutrons, on the other hand, interact with nuclei through the strong nuclear force, which is highly local. Inelastic scattering of neutrons, which is the basis of INS spectroscopy, is strongly dependent on the nuclear spin and is particularly strong for protons.

In systems with pairs of protons exhibiting *ortho–para* spin isomerism (H_2 and H_2O), the neutron scattering amplitudes depend strongly on the total nuclear spin quantum numbers of the initial and final states. The INS is weak for *para–para* transitions, since both the initial and final states have nuclear spin $I = 0$, while it is relatively strong for *ortho–ortho* transitions, where both initial and final states have spin $I = 1$. Very importantly, inelastic scattering is also strong for *ortho–para* transitions, in which the total nuclear spin quantum number changes from 1 to 0, or vice versa. INS spectroscopy therefore allows the direct detection of *ortho–para* transitions and allows the *ortho* and *para* levels to be aligned on the energy level diagram.

At low temperature, the presence of a neutron energy gain peak is often a characteristic signature of the presence of metastable spin isomers. For example, the neutron energy gain peak at $\Delta E = -14.7$ meV in figure 9 derives from H_2 molecules in the *ortho*-H_2 ground state depositing energy in the scattered neutrons and ending up in the *para*-H_2 ground state [49]. The existence of this peak at a sample temperature of 1.6 K is inconsistent with a sample in complete thermal equilibrium, since 14.7 meV corresponds to $\Delta E/k_B = 170$ K, where k_B is the Boltzmann

Downloaded from rsta.royalsocietypublishing.org on August 12, 2013

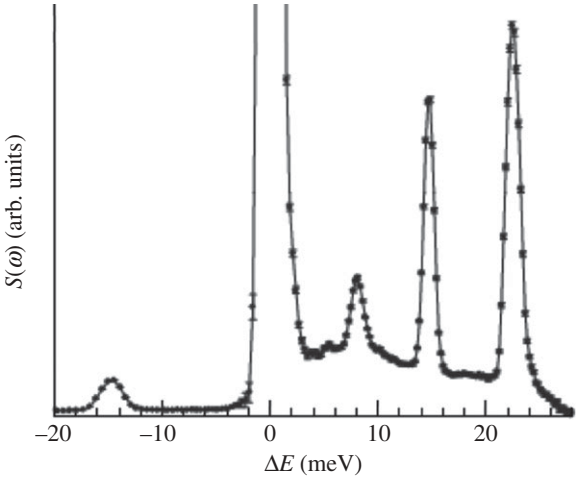

Figure 9. Inelastic neutron scattering spectrum of $H_2@C_{60}$ at a temperature of 1.6 K. The neutron energy gain peak at $\Delta E = -14.7$ meV is a signature of metastable *ortho*-H_2. Adapted with permission of the American Physical Society from Horsewill *et al.* [49].

constant, which far exceeds the sample temperature. The neutron energy gain peak is due to a large proportion of H_2 molecules trapped in a metastable high-energy *ortho*-H_2 state by the poor efficiency of *ortho–para* conversion.

A low-temperature neutron energy gain peak is also observed for $H_2O@C_{60}$, indicating the metastable trapping of the endohedral *ortho*-H_2O spin isomer [56].

It is possible to study the neutron momentum transfer spectrum as well as the change in neutron energy. Momentum transfer studies provide information on the physical dimensions of the scattering object. The neutron momentum transfer spectra of H_2 endofullerenes are consistent with the known size of the H_2 molecule and the spread of the confined molecular wave function [48,49].

(d) Nuclear magnetic resonance: solution nuclear magnetic resonance

(i) Chemical shifts of the endofullerene molecules

Solution NMR is the primary physical method for the basic characterization of small-molecule endofullerenes. The fullerene cage has a significant magnetic shielding effect on the endofullerene atoms or molecules, leading in most cases to negative chemical shifts δ for the endohedral species. These unusual chemical shifts render solution NMR a highly diagnostic characterization method for endofullerenes.

The proton chemical shifts for the dihydrogen endofullerenes $H_2@C_{60}$ and $H_2@C_{70}$ are -5.9 ppm and -28.5 ppm, respectively, both relative to free H_2 [22,24]. The proton chemical shift for $H_2O@C_{60}$ is shifted by -6.2 ppm relative to free H_2O in the same solvent [23]. The ^{3}He chemical shifts of the noble gas endofullerenes $^3He@C_{60}$ and $^3He@C_{70}$ are -6.4 ppm and -28.8 ppm relative to free ^{3}He, respectively [9,11]. The similarity of the endohedral chemical shifts for ^{3}He, H_2 and H_2O is consistent with the electronic structure of the cage being only weakly perturbed by the endohedral species.

The stronger magnetic shielding by the C_{70} cage, relative to the C_{60} cage, may be rationalized by noting that six-membered rings have a shielding effect (negative contributions to δ), while five-membered rings deshield (positive contributions to δ). These two effects partially compensate in C_{60}, leading to a relatively small negative chemical shift. Since C_{70} contains more six-membered rings than does C_{60}, but the same number of five-membered rings, the resultant shielding effect

Downloaded from rsta.royalsocietypublishing.org on August 12, 2013

is stronger (more negative δ). Similarly, endohedral shifts are often larger in open C_{60} than in closed C_{60} species, since the compensation of six-membered and five-membered rings is disrupted [20,21].

The fully reduced C_{60}^{6-} fullerene cage generates a very strong shielding effect, so that the ^{3}He resonance peak in the $^3He@C_{60}^{6-}$ anion is at the extreme chemical shift of −48.7 ppm, relative to ^{3}He gas in solution [37]. The C_{70}^{6-} anion, on the other hand, has a net deshielding effect, providing a ^{3}He chemical shift in $^3He@C_{70}^{6-}$ of +8.3 ppm, relative to ^{3}He gas in solution [37].

The ^{3}He chemical shift in the 'molecular' endofullerene $^3He_2@C_{70}$ is shifted by 0.014 ppm in the direction of positive δ (lower shielding) relative to $^3He@C_{70}$ [13]. Similarly, the proton chemical shift in the two-molecule endofullerene $2H_2@C_{70}$ is shifted by 0.17 ppm in the direction of positive δ (lower shielding) relative to $H_2@C_{70}$ [24]. These small differences between endofullerenes with one or two encapsulated species may be rationalized by postulating that the centre of the C_{70} cage is more highly shielded than the periphery. When the cage contains two atoms or molecules, steric crowding forces the endohedral species to spend more time away from the cage centre, and hence in a slightly less shielded region.

The chemical shift differences between ^{3}He and $^3He_2$ endofullerenes have also been studied in species with reduced fullerene cages of the form C_{60}^{6-} and C_{70}^{6-}. There is a positive δ shift of 0.093 ppm for $^3He_2@C_{60}^{6-}$ relative to $^3He@C_{60}^{6-}$, but a negative δ shift of −0.154 ppm for $^3He_2@C_{70}^{6-}$ relative to $^3He@C_{70}^{6-}$ [15]. The change in sign is attributed to internal magnetic field distributions with opposite polarity for C_{60}^{6-} and C_{70}^{6-} [15].

A remarkable example is provided by an open-cage variant of the bimolecular endofullerene $2H_2@C_{70}$ [58]. In this case, the open-cage fullerene is asymmetric, so that the shielding is different at one end of the cage from the other. At low temperature, the two endohedral H_2 molecules occupy inequivalent locations within the cage and experience different chemical shifts, giving two NMR peaks in solution NMR. However, at high temperature, the two endohedral molecules rapidly exchange places, providing a single NMR peak at the average chemical shift [58].

(ii) Chemical shifts of the cage nuclei

The ^{13}C chemical shifts of the fullerene cages are slightly influenced by the presence of the endohedral molecules, indicating a very weak perturbation of the cage electrons by the endohedral species. For example, the ^{13}C resonance of $H_2@C_{60}$ is shifted by 0.078 ppm in the direction of positive δ, relative to that of C_{60} [22]. Similarly, the ^{13}C resonance of $H_2O@C_{60}$ is shifted by 0.11 ppm in the direction of positive δ, relative to that of C_{60} [23]. At the time of writing, there is no evidence that *ortho* and *para* endohedral species induce different ^{13}C chemical shift changes in the cage.

(iii) Spin–spin couplings

The solution NMR of endohedral HD or HDO species reveals spin–spin couplings between the ^{1}H and ^{2}H nuclei. For example, the ^{1}H spectrum of $HD@C_{60}$ is a 1 : 1 : 1 triplet reflecting the three magnetic quantum states $m_I \in \{-1, 0, +1\}$ of the spin $I = 1$ deuterium nucleus [35,36,38, 54,55,91]. The ^{2}H atom also induces a secondary isotope shift of approximately 0.02 ppm for the neighbouring ^{1}H nucleus. As a result, the solution-state ^{1}H NMR spectrum of a mixture of $HD@C_{60}$ and $H_2@C_{60}$ contains four resolved peaks in the endohedral region of the spectrum: three for $HD@C_{60}$ and one for $H_2@C_{60}$ (figure 10). No spin–spin couplings have been observed between the nuclei of endohedral species and cage nuclei, by solution NMR.

(iv) *Ortho–para* conversion

In an elegant series of experiments, the group of Turro showed that the HD peaks of a $HD@C_{60}/H_2@C_{60}$ mixture serve as an unambiguous amplitude reference, facilitating the NMR detection of *ortho–para* conversion in $H_2@C_{60}$ [35,36,38,54,55,92]. Solutions were prepared in which $H_2@C_{60}$ was enriched in *para*-H_2 and depleted in *ortho*-H_2 (see below). Such samples

Downloaded from rsta.royalsocietypublishing.org on August 12, 2013

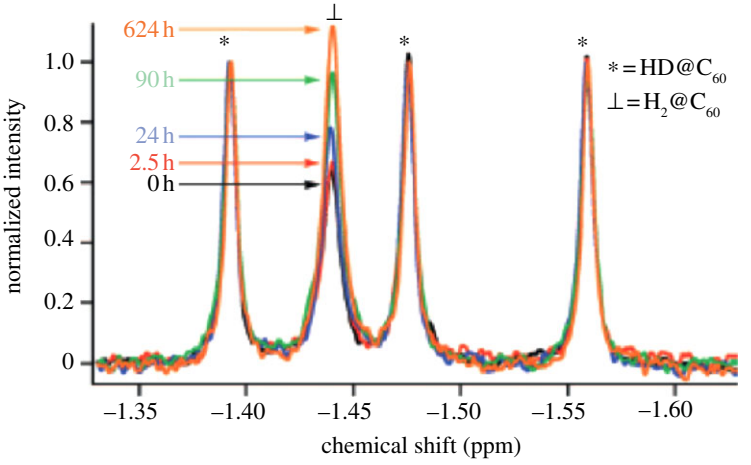

Figure 10. Endohedral region of the 500 MHz ^{1}H NMR spectrum of a mixture of $H_2@C_{60}$ and $HD@C_{60}$, dissolved in 1,2-dichlorobenzene-d_4. Three peaks are assigned to $HD@C_{60}$, and one peak to $H_2@C_{60}$, as indicated. The sample was enriched in the *para* spin isomer of H_2 by low-temperature exposure to O_2, and redissolved. The growth in the $H_2@C_{60}$ peak as a function of time indicates the slow reconversion of *para*-H_2 to *ortho*-H_2. Adapted with permission from Turro *et al.* [55]. Copyright 2008 American Chemical Society. (Online version in colour.)

provide relatively weak NMR signals, since the *para*-H_2 species has no nuclear spin and does not generate an NMR signal. As spin-isomer conversion proceeds, the proportion of *ortho*-H_2 recovers back to its thermal equilibrium value, and the NMR signal intensity recovers. This intensity change is easily seen by observing the HD peaks at the same time (figure 10).

In order to perform such experiments, protocols were developed for enriching samples in the *para*-H_2 spin isomer, and for inducing spin-isomer conversion in a room-temperature solution. The *para*-H_2 enrichment was performed by dispersing $H_2@C_{60}$ on the surface of a zeolite, which was then immersed in liquid O_2 at 77 K [55]. The paramagnetic O_2 acts as an efficient low-temperature catalyst for the spin-isomer conversion. At 77 K, the equilibrium *ortho* : *para* ratio is about 1 : 1. The oxygen is rapidly removed as the sample is raised to room temperature and dissolved, trapping the molecules in a non-equilibrium state with an enhanced percentage of *para*-H_2. After dissolution, the equilibration of the spin isomers is induced by dissolved paramagnetic species such as oxygen or stable nitroxide radicals [55]. These species induce a slow recovery of the *ortho* : *para* ratio to the room-temperature thermal equilibrium value of about 3 : 1. The *ortho*-H_2 NMR signals therefore gradually increase as equilibrium is re-established (figure 10).

It is also possible to induce spin-isomer conversion by nitroxide radicals attached to the exterior of the fullerene cage [92]. The *ortho–para* conversion could be controlled by chemical reactions of the attached radical [35]. Illumination of the fullerene cages by a strong lamp induces spin-isomer conversion through the generation of photo-excited electronic triplet states of the fullerene cage. The photo-induced spin-isomerization process is much more efficient for $H_2@C_{70}$ than for $H_2@C_{60}$, in part because the photo-excited triplet lifetimes are longer for C_{70} [38].

(v) Spin–lattice relaxation

The proton spin relaxation in $H_2@C_{60}$ has been compared with that of free H_2 in solution [50,91]. The temperature dependence of the spin relaxation was modelled using a superposition of dipole–dipole and spin–rotation mechanisms.

(e) Solid-state nuclear magnetic resonance

Solid-state NMR provides access to a much wider range of temperatures than solution NMR. In particular, solid-state NMR may be conducted at cryogenic temperatures, where the rotational

Downloaded from rsta.royalsocietypublishing.org on August 12, 2013

state quantization of the endohedral molecular rotors provides a range of interesting phenomena. Some of the familiar concepts of everyday NMR break down in the cryogenic regime. For example, molecules can no longer be described using concepts of point-like nuclei with well-defined locations. Endohedral molecular fullerenes provide well-controlled examples for advancing the understanding of NMR in spatially quantized systems—and hopefully, for putting such spin-space entanglement effects to good use.

Spin isomerism is a prominent phenomenon in the NMR of rotating molecules and molecular groups at low temperature. For example, rotating methyl groups also display spin isomerism, and the entanglement of the spatial and spin degrees of freedom gives rise to potentially useful physical effects, such as the generation of enhanced nuclear spin order by a change in sample temperature [93–96]. A similar phenomenon is anticipated for systems such as $H_2@C_{60}$ and $H_2O@C_{60}$, but this has not been observed, at the time of writing.

(i) Intramolecular dipole–dipole couplings

The proton nuclei in H_2 and H_2O interact through the proximity of their magnetic moments (the dipole–dipole coupling mechanism) [77]. In the NMR of isotropic solutions, this magnetic dipole–dipole coupling interaction is averaged to zero through the isotropic molecular tumbling. However, in anisotropic media such as solids, the dipole–dipole coupling generates spectral splittings and other spin-dynamical phenomena.

Dipole–dipole couplings within the endohedral molecules were first observed for an open-cage variant of $H_2@C_{60}$, in which the cage is strongly asymmetric [51]. In this study, magic-angle-spinning NMR was used to obtain sufficient spectral resolution to resolve the endohedral proton peaks in the solid state. Since magic angle spinning averages out dipolar couplings, a double-quantum radiofrequency recoupling method was applied in order to observe the couplings in the form of signal modulations. Dipolar couplings were measured in the temperature range from 120 to 300 K. These were consistent with hydrogen molecules executing a slightly anisotropic rotational motion within the asymmetric cage [51].

Technical advances have made it possible to perform magic-angle-spinning NMR in the cryogenic regime. This allows the NMR study of endohedral molecules occupying small numbers of rotational/translational quantum states. Figure 11*d* shows the magic-angle-spinning proton NMR spectrum of $H_2O@C_{60}$ at a sample temperature of 9.6 K [56]. The sideband structure in the proton spectrum is consistent with a proton–proton dipole–dipole coupling having a magnitude of about 5.5 kHz [56]. The existence of this coupling is a surprise, since the icosahedral environment provided by the C_{60} cage is expected to eliminate such interactions. The observation of this coupling, combined with spectroscopic evidence from neutron scattering, indicates that the symmetry is broken and the degeneracy lifted in the rotational ground state of *ortho*-water in $H_2O@C_{60}$ [56]. The origin of the symmetry breaking is not yet known.

The interpretation of interactions such as dipole–dipole couplings requires care for systems displaying spatial quantization. In high-temperature NMR, the dipole–dipole coupling between two nuclei with magnetogyric ratios γ_j and γ_k is usually interpreted in terms of the dipole–dipole coupling constant $b_{jk} = -(\mu_0/4\pi)\gamma_j\gamma_k\hbar r_{jk}^{-3}$, where μ_0 is the magnetic constant and r_{jk} is the distance between the spins [77]. This formulation is appropriate for point nuclei, but is not applicable to delocalized spatial wave functions such as those encountered in the NMR of endofullerenes. For example, consider the direct dipole–dipole coupling between the two proton nuclei in an H_2 molecule. The internuclear distance in H_2 is about 74 pm, which would correspond to a dipole–dipole coupling of −309 kHz, if the nuclei were highly localized. In fact, the hydrogen molecule is described by a delocalized quantum wave function, and the spatial spread of the wave function strongly reduces the magnitude of anisotropic nuclear spin interactions. For example, in the case where the hydrogen molecule occupies the single rotational quantum state $|J, M_J\rangle = |1, 0\rangle$, the dipole–dipole coupling has a magnitude given by the localized value, but multiplied by a factor of 2/5 [41,51,97,98]. Similarly, the dipolar scaling factor for the $|J, M_J\rangle = |1, +1\rangle$ state is −1/5. These are large factors, which can cause serious errors in interpretation if ignored.

Downloaded from rsta.royalsocietypublishing.org on August 12, 2013

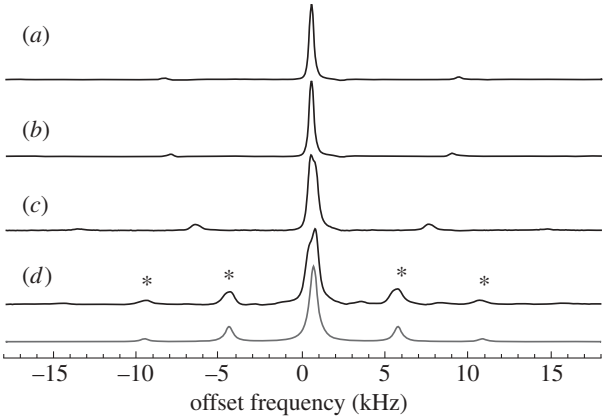

Figure 11. Magic-angle-spinning proton NMR spectra of $H_2O@C_{60}$, at a proton resonance frequency of 600.0 MHz. The sample temperatures are (*a*) 22.8 K, (*b*) 18.5 K, (*c*) 13.0 K and (*d*) 9.6 K. The spinning sidebands (indicated by asterisks) are generated by a finite dipole–dipole coupling between the water protons. The grey line is a simulation for randomly oriented proton pairs with a dipole–dipole coupling of −5.5 kHz. The existence of these dipole–dipole couplings indicates a lifting of the degeneracy in the *ortho*-H_2O ground state, a conclusion that is supported by neutron scattering data. Adapted with permission from Beduz *et al.* [56].

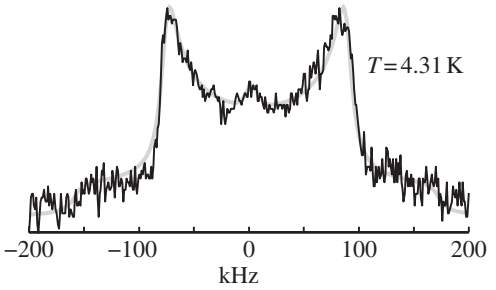

Figure 12. Proton spectrum of $H_2@ATOCF$ at a temperature of 4.31 K (ATOCF denotes an open-cage thia-aza fullerene). The spectral lineshape matches well with the Pake pattern predicted for randomly oriented proton pairs (grey line, simulation). The magnitude of the dipolar coupling agrees with the theoretical dipolar coupling for a hydrogen molecule in the non-degenerate rotational ground state $|J, M\rangle = |1, 0\rangle$, assuming that the quantization axis is fixed with respect to the asymmetric open cage and is randomly oriented in a powder. Adapted with permission from Carravetta *et al.* [28]. Copyright 2006, American Institute of Physics.

Figure 12 shows the low-temperature proton NMR spectrum of an open-cage variant of $H_2@C_{60}$ with low cage symmetry [28]. The proton NMR signals are generated by metastable ortho-hydrogen molecules in the $J = 1$ rotational ground state. The three states with $M_J \in \{-1, 0, +1\}$ are degenerate in a symmetrical environment but the degeneracy is lifted by the asymmetric rotational potential (figure 7). At 4.2 K, all *ortho*-H_2 molecules occupy the state of lowest energy, which is $|J, M_J\rangle = |1, 0\rangle$, where the quantization axis corresponds to one of the principal axes of the quadratic cage potential. As discussed earlier, the dipole–dipole coupling tensor in this state is oriented with respect to the cage, and scaled in magnitude by a factor of 2/5 with respect to the case of localized nuclei. A powder sample contains a large number of cages with random orientations, so the NMR spectrum takes the form of the classic 'Pake pattern' [99], with a splitting between the 'horns' of 3/2 times the dipolar coupling constant [77]. The predicted spectral splitting is 185 kHz, on the basis of the 74 pm internuclear distance in H_2, and taking into account the 2/5 delocalization factor. This theoretical prediction is in good agreement with

Downloaded from rsta.royalsocietypublishing.org on August 12, 2013

the observed splitting in the spectrum shown in figure 12, which is approximately 175 kHz. The remaining discrepancy is attributed to the vibrational zero-point motion, which also reduces the dipole–dipole coupling.

At higher temperatures, more rotational states are excited. The nuclear spin system experiences the thermal average of the spin interactions, taken over all occupied quantum states. Since some of the rotational states have dipolar coupling tensors with opposite signs, thermal averaging leads to a reduction in the magnitude of the dipole–dipole coupling. At high temperature, when a large number of rotational levels are occupied approximately equally, the dipole–dipole coupling tensor vanishes. This phenomenon corresponds to a quantum version of isotropic molecular tumbling. By tracking the dipole–dipole coupling constant as a function of temperature, it is possible to validate models of the rotational energy level structure [28].

Dipole–dipole couplings between the endohedral protons are not anticipated in $H_2@C_{60}$ and $H_2O@C_{60}$, since the icosahedral cage symmetry leads to quantum states with vanishing matrix elements for second-rank tensors. Despite this expectation, such couplings are clearly observed for $H_2O@C_{60}$, as evidenced by the magic-angle-spinning spectra shown in figure 11 [56].

In the case of $H_2@C_{60}$, spectral features associated with intramolecular dipole–dipole couplings appear for some samples at low temperatures, but not for others [43]. The low-temperature behaviour of $H_2@C_{60}$ appears to be sensitive to the sample purity and solid-state preparation. This topic is under investigation.

Observation of the intramolecular dipole–dipole couplings between the protons of $H_2@C_{70}$ are consistent with magnetic orientation of the long axes of the carbon cages at low temperature [53].

(ii) Spin–rotation couplings

Molecular beam spectra of *ortho*-H_2 and *ortho*-H_2O display spectral structure associated with couplings between the nuclear spin angular momentum and the rotational angular momentum of the molecule [79]. In the NMR of gases and liquids, collisions modulate these couplings, which become a significant relaxation mechanism [82,100]. However, resolved spectral structure generated by coherent spin–rotation couplings have never been observed in bulk NMR, to the knowledge of the author, although the spectral consequences of such couplings have been analysed in a related context [97,98]. The protected environment inside a fullerene cage is a promising environment for the generation of coherent spin–rotation couplings. Nevertheless, at the time of writing, spectral evidence of coherent spin–rotation couplings has not been observed for molecular endofullerenes.

(iii) Intermolecular dipole–dipole couplings

Solid-state NMR experiments demonstrate the existence of dipolar couplings between nuclei of the endohedral molecules and nuclei within the cage, or outside it. For example, cross-polarization experiments have been performed in which nuclear angular momentum is transferred, via dipolar couplings, from the protons of endohedral H_2 to ^{13}C nuclei in the fullerene cage [39]. Spherical tensor analysis of the proton NMR response in solid $H_2@C_{60}$ has shown that protons in neighbouring cages have a significant mutual coupling [39]. In magic-angle-spinning NMR experiments, a study of spin–lattice relaxation times as a function of spinning frequency has shown that fast-relaxing endohedral protons can act as relaxation sinks for exohedral protons. The endohedral and exohedral protons interact through dipolar couplings [39].

(iv) Isotropic chemical shifts

Isotropic chemical shifts may be measured in the solid state by using magic angle spinning to average out anisotropic interactions such as chemical shift anisotropies and dipole–dipole couplings, which otherwise degrade the spectral resolution [101]. So far, all isotropic chemical shifts observed in the solid state are similar to the solution-state values. For example, the

Downloaded from rsta.royalsocietypublishing.org on August 12, 2013

solid-state ^{13}C spectrum of $H_2@C_{60}$ displays a single peak in the magic-angle-spinning NMR at room temperature, while open-cage and exohedrally modified variants display numerous ^{13}C peaks, due to the broken cage symmetry [39].

(v) Chemical shift anisotropy

The ^{13}C sites in C_{60} cages experience a large (approx. 180 ppm) chemical shift anisotropy (CSA) interaction, generated by the diamagnetic currents in the conjugated rings. This CSA interaction gives rise to a very broad 'powder pattern' spectral peak for ^{13}C at low temperatures (less than approx. 100 K) [64]. At high temperature (more than approx. 170 K), the ^{13}C CSA is averaged out by rapid large-angle orientational jumps of the cages, giving a single narrow peak in the ^{13}C NMR spectrum [64]. At intermediate temperatures, the broad and narrow peaks coexist, suggesting distinct solid-state domains with slightly different rotational barriers. Similar behaviour is observed in the ^{13}C NMR of $H_2@C_{60}$ [39].

In pure C_{60}, the modulation of the CSA tensor by rotational motion of the cages drives ^{13}C spin–lattice relaxation, characterized by the time constant T_1. A distinct change in the ^{13}C spin–lattice relaxation behaviour is observed at approximately 263 K, corresponding to the first-order phase transition of the crystal structure, which marks a change from isotropic tumbling of the cages (above the phase transition) to large-amplitude jump motions (below the phase transition) [64]. The ^{13}C spin–lattice relaxation of solid $H_2@C_{60}$ behaves in a similar way, but with a transition in T_1 at the lower temperature of approximately 235 K [39]. It is not yet known if this temperature corresponds to the thermodynamic phase transition in $H_2@C_{60}$.

5. Concluding remarks

The de novo synthesis of small-molecule endofullerenes is an outstanding feat of synthetic chemistry and has provided a focal point for several different forms of physical measurements, advanced synthetic techniques and various levels of quantum theory. A full understanding of these systems can only be achieved by a detailed collaboration between researchers using many different physical techniques, acting in concert with synthetic chemists to generate new systems for the validation and testing of theories. A recent paper on $H_2O@C_{60}$ has 22 co-authors and involves a collaboration between eight research groups in five different countries [56]. This is not an artificial construction generated by the demands of funding organizations, but has arisen spontaneously out of the complementary interests of many different scientists studying the same physical system.

The search for understanding of the quantum behaviour of molecular endofullerenes is not purely driven by academic interest. These substances may have useful physical properties. Hydrogen storage applications come to mind but are unrealistic due to the low energy density and the difficulty of releasing the encapsulated hydrogen. Nevertheless, the study of hydrogen endofullerenes is leading to an improved understanding of the interaction between hydrogen molecules and curved carbon surfaces, and this may have long-term applications to energy research.

Unusual material properties are anticipated for some endofullerenes. A crystal of $H_2O@C_{60}$ provides a three-dimensional array of freely rotating electric dipoles, coupled by a through-space electric dipole coupling. Cooperative properties such as ferroelectricity are anticipated for materials of this kind [61].

The light-controlled switching of endofullerene spin isomers suggests distant applications to quantum information processing [38].

Molecular endofullerenes provide systems displaying a controlled interplay of molecular angular momentum, nuclear spin quantization and spin isomerism. Systems of this kind have potential as novel agents for generating nuclear spin hyperpolarization, complementary to the dynamic nuclear polarization and parahydrogen-induced polarization techniques, which are widely used for enhancing NMR signals in the condensed phase [102–106]. There is a

Downloaded from rsta.royalsocietypublishing.org on August 12, 2013

clear relationship between spin-isomer conversion in endofullerenes and nuclear singlet–triplet conversion, a central topic in singlet NMR [107].

Acknowledgements. The author would particularly like to acknowledge the insightful contributions of Salvatore Mamone provided over many fruitful discussions, and the detailed comments on the manuscript by Toomas Rõõm. Many other collaborators including Marina Carravetta, Tony Horsewill, Nick Turro and Ron Lawler have also contributed fine insights. I would also like to thank Koichi Komatsu, Yasujiro Murata, Nick Turro and their co-workers for providing samples for use in our group. I also thank Andrea Krachmalnicoff for help with figure 1.

Funding statement. This work was supported by the EPSRC (UK), the Royal Society (UK), the Leverhulme Trust (UK) and the European Research Council.

References

1. Kroto HW, Heath JR, O'Brien SC, Curl RF, Smalley RE. 1985 C_{60}: buckminsterfullerene. *Nature* **318**, 162–163. (doi:10.1038/318162a0)
2. Chai Y, Guo T, Jin CM, Haufler RE, Chibante LPF, Fure J, Wang LH, Alford JM, Smalley RE. 1991 Fullerenes with metals inside. *J. Phys. Chem.* **95**, 7564–7568. (doi:10.1021/j100173a002)
3. Rodriguez-Fortea A, Balch AL, Poblet JM. 2011 Endohedral metallofullerenes: a unique host–guest association. *Chem. Soc. Rev.* **40**, 3551–3563. (doi:10.1039/c0cs00225a)
4. Akasaka T, Nagase S. 2002 *Endofullerenes: a new family of carbon clusters*. Dordrecht, The Netherlands: Kluwer Academic.
5. Yamada M, Akasaka T, Nagase S. 2011 New vistas in endohedral metallofullerenes. In *Handbook of carbon nano materials*, vol. 1, *Synthesis and supramolecular systems* (eds F D'Souza, KM Kadish), pp. 145–183. Singapore: World Scientific.
6. Stevenson S *et al.* 1999 Small-bandgap endohedral metallofullerenes in high yield and purity. *Nature* **401**, 55–57. (doi:10.1038/43415)
7. Stevenson S. 2011 Metallic oxide clusters in fullerene cages. In *Handbook of carbon nano materials*, vol. 1, *Synthesis and supramolecular systems* (eds F D'Souza, KM Kadish), pp. 185–205. Singapore: World Scientific.
8. Krätschmer W, Fostiropoulos K, Huffman DR. 1990 The infrared and ultraviolet absorption spectra of laboratory-produced carbon dust: evidence for the presence of the C_{60} molecule. *Chem. Phys. Lett.* **170**, 167–170. (doi:10.1016/0009-2614(90)87109-5)
9. Saunders M, Cross RJ, Jimenez-Vazquez HA, Shimshi R, Khong A. 1996 Noble gas atoms inside fullerenes. *Science* **271**, 1693–1697. (doi:10.1126/science.271.5256.1693)
10. Saunders M, Jimenez-Vazquez HA, Cross RJ, Poreda RJ. 1993 Stable compounds of helium and neon: He@C_{60} and Ne@C_{60}. *Science* **259**, 1428–1430. (doi:10.1126/science.259.5100.1428)
11. Saunders M, Jimenez-Vazquez HA, Cross RJ, Mroczkowski S, Freedberg DI, Anet FAL. 1994 Probing the interior of fullerenes by ^{3}He NMR spectroscopy of endohedral ^{3}He@C_{60} and ^{3}He@C_{70}. *Nature* **367**, 256–258. (doi:10.1038/367256a0)
12. Becker L, Poreda RJ, Bunch TE. 2000 Fullerenes: an extraterrestrial carbon carrier phase for noble gases. *Proc. Natl Acad. Sci. USA* **97**, 2979–2983. (doi:10.1073/pnas.97.7.2979)
13. Khong A, Jiménez-Vázquez HA, Saunders M, Cross RJ, Laskin J, Peres T, Lifshitz C, Strongin R, Smith AB. 1998 An NMR study of He_2 inside C_{70}. *J. Am. Chem. Soc.* **120**, 6380–6383. (doi:10.1021/ja980142h)
14. Laskin J, Peres T, Lifshitz C, Saunders M, Cross RJ, Khong A. 1998 An artificial molecule of Ne_2 inside C_{70}. *Chem. Phys. Lett.* **285**, 7–9. (doi:10.1016/s0009-2614(97)01473-5)
15. Sternfeld T, Hoffman RE, Saunders M, Cross RJ, Syamala MS, Rabinovitz M. 2002 Two helium atoms inside fullerenes: probing the internal magnetic field in C_{60}^{6-} and C_{70}^{6-}. *J. Am. Chem. Soc.* **124**, 8786–8787. (doi:10.1021/ja025990y)
16. Almeida Murphy T, Pawlik T, Weidinger A, Höhne M, Alcala R, Spaeth JM. 1996 Observation of atomlike nitrogen in nitrogen-implanted solid C_{60}. *Phys. Rev. Lett.* **77**, 1075–1078. (doi:10.1103/PhysRevLett.77.1075)
17. Knapp C, Weiden N, Käss K, Dinse KP, Pietzak B, Waiblinger M, Weidinger A. 1998 Electron paramagnetic resonance study of atomic phosphorus encapsulated in [60]fullerene. *Mol. Phys.* **95**, 999–1004. (doi:10.1080/00268979809483233)

Downloaded from rsta.royalsocietypublishing.org on August 12, 2013

18. Cao BP, Peres T, Cross RJ, Saunders M, Lifshitz C. 2001 Do nitrogen-atom-containing endohedral fullerenes undergo the shrink-wrap mechanism? *J. Phys. Chem. A* **105**, 2142–2146. (doi:10.1021/jp001359c)
19. Ito S, Shimotani H, Takagi H, Dragoe N. 2008 On the synthesis conditions of N and N_2 endohedral fullerenes. *Fullerenes, Nanotubes Carbon Nanostruct.* **16**, 206–213. (doi:10.1080/15363830802064187)
20. Rubin Y, Jarrosson T, Wang G-W, Bartberger MD, Houk KN, Schick G, Saunders M, Cross RJ. 2001 Insertion of helium and molecular hydrogen through the orifice of an open fullerene. *Angew. Chem. Int. Edn.* **40**, 1543–1546. (doi:10.1002/1521-3773(20010417)40:8<1543::AID-ANIE1543>3.0.CO;2-6)
21. Murata Y, Murata M, Komatsu K. 2003 100% encapsulation of a hydrogen molecule into an open-cage fullerene derivative and gas-phase generation of $H_2@C_{60}$. *J. Am. Chem. Soc.* **125**, 7152–7153. (doi:10.1021/ja0354162)
22. Komatsu K, Murata M, Murata Y. 2005 Encapsulation of molecular hydrogen in fullerene C_{60} by organic synthesis. *Science* **307**, 238–240. (doi:10.1126/science.1106185)
23. Kurotobi K, Murata Y. 2011 A single molecule of water encapsulated in fullerene C_{60}. *Science* **333**, 613–616. (doi:10.1126/science.1206376)
24. Murata M, Maeda S, Morinaka Y, Murata Y, Komatsu K. 2008 Synthesis and reaction of fullerene C_{70} encapsulating two molecules of H_2. *J. Am. Chem. Soc.* **130**, 15 800–15 801. (doi:10.1021/ja8076846)
25. Iwamatsu S, Stanisky CM, Cross RJ, Saunders M, Mizorogi N, Nagase S, Murata S. 2006 Carbon monoxide inside an open-cage fullerene. *Angew. Chem. Int. Edn.* **45**, 5337–5340. (doi:10.1002/anie.200601241)
26. Whitener KE, Cross RJ, Saunders M, Iwamatsu S, Murata S, Mizorogi N, Nagase S. 2009 Methane in an open-cage [60]fullerene. *J. Am. Chem. Soc.* **131**, 6338–6339. (doi:10.1021/ja901383r)
27. Whitener KE, Frunzi M, Iwamatsu S-I, Murata S, Cross RJ, Saunders M. 2008 Putting ammonia into a chemically opened fullerene. *J. Am. Chem. Soc.* **130**, 13 996–13 999. (doi:10.1021/ja805579m)
28. Carravetta M, Johannessen OG, Levitt MH, Heinmaa I, Stern R, Samoson A, Horsewill AJ, Murata Y, Komatsu K. 2006 Cryogenic NMR spectroscopy of endohedral hydrogen–fullerene complexes. *J. Chem. Phys.* **124**, 104507. (doi:10.1063/1.2174012)
29. Horsewill AJ *et al.* 2010 Inelastic neutron scattering of a quantum translator–rotator encapsulated in a closed fullerene cage: isotope effects and translation–rotation coupling in $H_2@C_{60}$ and $HD@C_{60}$. *Phys. Rev. B* **82**, 081410. (doi:10.1103/PhysRevB.82.081410)
30. Ge M *et al.* 2011 Interaction potential and infrared absorption of endohedral H_2 in C_{60}. *J. Chem. Phys.* **134**, 054507. (doi:10.1063/1.3535598)
31. Nairz O, Arndt M, Zeilinger A. 2003 Quantum interference experiments with large molecules. *Am. J. Phys.* **71**, 319–325. (doi:10.1119/1.1531580)
32. Iwamatsu SI, Uozaki T, Kobayashi K, Re S, Nagase S, Murata S. 2004 A bowl-shaped fullerene encapsulates a water into the cage. *J. Am. Chem. Soc.* **126**, 2668–2669. (doi:10.1021/ja038537a)
33. Bingel C. 1993 Cyclopropanierung von Fullerenen. *Chem. Ber.* **126**, 1957–1959. (doi:10.1002/cber.19931260829)
34. Maggini M, Scorrano G, Prato M. 1993 Addition of azomethine ylides to C_{60}: synthesis, characterization, and functionalization of fullerene pyrrolidines. *J. Am. Chem. Soc.* **115**, 9798–9799. (doi:10.1021/ja00074a056)
35. Li Y *et al.* 2010 A magnetic switch for spin-catalyzed interconversion of nuclear spin isomers. *J. Am. Chem. Soc.* **132**, 4042–4043. (doi:10.1021/ja910282p)
36. Sartori E, Ruzzi M, Lawler RG, Turro NJ. 2008 Nitroxide paramagnet-induced *para–ortho* conversion and nuclear spin relaxation of H_2 in organic solvents. *J. Am. Chem. Soc.* **130**, 12 752–12 756. (doi:10.1021/ja8037195)
37. Shabtai E *et al.* 1998 ^{3}He NMR of $He@C_{60}^{6-}$ and $He@C_{70}^{6-}$. New records for the most shielded and the most deshielded ^{3}He inside a fullerene. *J. Am. Chem. Soc.* **120**, 6389–6393. (doi:10.1021/ja9805831)
38. Frunzi M *et al.* 2011 A photochemical on–off switch for tuning the equilibrium mixture of H_2 nuclear spin isomers as a function of temperature. *J. Am. Chem. Soc.* **133**, 14 232–14 235. (doi:10.1021/ja206383n)

Downloaded from rsta.royalsocietypublishing.org on August 12, 2013

39. Carravetta M *et al.* 2007 Solid-state NMR of endohedral hydrogen–fullerene complexes. *Phys. Chem. Chem. Phys.* **9**, 4879–4894. (doi:10.1039/b707075f)
40. Kohama Y *et al.* 2009 Rotational sublevels of an ortho-hydrogen molecule encapsulated in an isotropic C_{60} cage. *Phys. Rev. Lett.* **103**, 073001. (doi:10.1103/PhysRevLett.103.073001)
41. Mamone S. 2012 Theory and spectroscopy of dihydrogen endofullerenes. PhD thesis, University of Southampton.
42. Mamone S *et al.* 2009 Rotor in a cage: infrared spectroscopy of an endohedral hydrogen–fullerene complex. *J. Chem. Phys.* **130**, 081103. (doi:10.1063/1.3080163)
43. Mamone S, Chen JYC, Bhattacharyya R, Levitt MH, Lawler RG, Horsewill AJ, Rõõm T, Bačić Z, Turro NJ. 2011 Theory and spectroscopy of an incarcerated quantum rotor: the infrared spectroscopy, inelastic neutron scattering and nuclear magnetic resonance of $H_2@C_{60}$ at cryogenic temperature. *Coord. Chem. Rev.* **255**, 938–948. (doi:10.1016/j.ccr.2010.12.029)
44. Cross RJ. 2001 Does H_2 rotate freely inside fullerenes? *J. Phys. Chem. A* **105**, 6943–6944. (doi:10.1021/jp011054d)
45. Xu M, Sebastianelli F, Bačić Z, Lawler R, Turro NJ. 2008 H_2, HD, and D_2 inside C_{60}: coupled translation–rotation eigenstates of the endohedral molecules from quantum five-dimensional calculations. *J. Chem. Phys.* **129**, 064313. (doi:10.1063/1.2967858)
46. Xu M, Sebastianelli F, Bačić Z, Lawler R, Turro NJ. 2008 Quantum dynamics of coupled translational and rotational motions of H_2 inside C_{60}. *J. Chem. Phys.* **128**, 011101. (doi:10.1063/1.2828556)
47. Xu M, Sebastianelli F, Gibbons BR, Bačić Z, Lawler R, Turro NJ. 2009 Coupled translation–rotation eigenstates of H_2 in C_{60} and C_{70} on the spectroscopically optimized interaction potential: effects of cage anisotropy on the energy level structure and assignments. *J. Chem. Phys.* **130**, 224306. (doi:10.1063/1.3152574)
48. Horsewill AJ *et al.* 2009 Quantum translator–rotator: inelastic neutron scattering of dihydrogen molecules trapped inside anisotropic fullerene cages. *Phys. Rev. Lett.* **102**, 013001. (doi:10.1103/PhysRevLett.102.013001)
49. Horsewill AJ *et al.* 2012 Inelastic neutron scattering investigations of the quantum molecular dynamics of a H_2 molecule entrapped inside a fullerene cage. *Phys. Rev. B* **85**, 205440. (doi:10.1103/PhysRevB.85.205440)
50. Sartori E, Ruzzi M, Turro NJ, Decatur JD, Doetschman DC, Lawler RG, Buchachenko AL, Murata Y, Komatsu K. 2006 Nuclear relaxation of H_2 and $H_2@C_{60}$ in organic solvents. *J. Am. Chem. Soc.* **128**, 14 752–14 753. (doi:10.1021/ja065172w)
51. Carravetta M *et al.* 2004 Solid state NMR of molecular hydrogen trapped inside an open-cage fullerene. *J. Am. Chem. Soc.* **126**, 4092–4093. (doi:10.1021/ja031536y)
52. Iwamatsu S-I, Murata S, Andoh Y, Minoura M, Kobayashi K, Mizorogi N, Nagase S. 2005 Open-cage fullerene derivatives suitable for the encapsulation of a hydrogen molecule. *J. Org. Chem.* **70**, 4820–4825. (doi:10.1021/jo050251w)
53. Mamone S *et al.* 2013 Nuclear magnetic resonance of hydrogen molecules trapped inside C_{70} fullerene cages. *ChemPhysChem*, accepted. (doi:10.1002/cphc.201300269)
54. Turro NJ *et al.* 2010 The spin chemistry and magnetic resonance of $H_2@C_{60}$. From the Pauli principle to trapping a long lived nuclear excited spin state inside a buckyball. *Acc. Chem. Res.* **43**, 335–345. (doi:10.1021/ar900223d)
55. Turro NJ *et al.* 2008 Demonstration of a chemical transformation inside a fullerene. The reversible conversion of the allotropes of $H_2@C_{60}$. *J. Am. Chem. Soc.* **130**, 10 506–10 507. (doi:10.1021/ja804311c)
56. Beduz C *et al.* 2012 Quantum rotation of *ortho* and *para*-water encapsulated in a fullerene cage. *Proc. Natl Acad. Sci. USA.* **109**, 12 894–12 898. (doi:10.1073/pnas.1210790109)
57. Iwamatsu S-I, Murata S. 2004 H_2O@open-cage fullerene C_{60}: control of the encapsulation property and the first mass spectroscopic identification. *Tetrahedron Lett.* **45**, 6391–6394. (doi:10.1016/j.tetlet.2004.07.008)
58. Murata Y, Maeda S, Murata M, Komatsu K. 2008 Encapsulation and dynamic behavior of two H_2 molecules in an open-cage C_{70}. *J. Am. Chem. Soc.* **130**, 6702–6703. (doi:10.1021/ja801753m)
59. Miyamoto Y, Fushitani M, Ando D, Momose T. 2008 Nuclear spin conversion of methane in solid parahydrogen. *J. Chem. Phys.* **128**, 114502. (doi:10.1063/1.2889002)
60. Bunker PR, Jensen P. 2006 *Molecular symmetry and spectroscopy*. Ottawa, Canada: NRC Research Press.
61. Cioslowski J, Nanayakkara A. 1992 Endohedral fullerites: a new class of ferroelectric materials. *Phys. Rev. Lett.* **69**, 2871–2873. (doi:10.1103/PhysRevLett.69.2871)

Downloaded from rsta.royalsocietypublishing.org on August 12, 2013

62. Meyer C, Harneit W, Lips K, Weidinger A, Jakes P, Dinse K-P. 2002 Alignment of the endohedral fullerenes N@C_{60} and N@C_{70} in a liquid-crystal matrix. *Phys. Rev. A* **65**, 061201. (doi:10.1103/PhysRevA.65.061201)
63. Dresselhaus MS, Dresselhaus G, Eklund PC. 1996 *Science of fullerenes and carbon nanotubes*. New York, NY: Academic Press.
64. Tycko R, Dabbagh G, Fleming RM, Haddon RC, Makhija AV, Zahurak SM. 1991 Molecular dynamics and the phase transition in solid C_{60}. *Phys. Rev. Lett.* **67**, 1886–1889. (doi:10.1103/PhysRevLett.67.1886)
65. Tycko R, Dabbagh G, Vaughan GBM, Heiney PA, Strongin RM, Cichy MA, Smith AB. 1993 Molecular orientational dynamics in solid C_{70}: investigation by one- and two-dimensional magic angle spinning nuclear magnetic resonance. *J. Chem. Phys.* **99**, 7554–7564. (doi:10.1063/1.465685)
66. Ge M *et al.* 2011 Infrared spectroscopy of endohedral HD and D_2 in C_{60}. *J. Chem. Phys.* **135**, 114511. (doi:10.1063/1.3637948)
67. FitzGerald SA, Churchill HOH, Korngut PM, Simmons CB, Strangas YE. 2006 Low-temperature infrared spectroscopy of H_2 in crystalline C_{60}. *Phys. Rev. B* **73**, 155409. (doi:10.1103/PhysRevB.73.155409)
68. Peng C, Stavola M, Fowler WB, Lockwood M. 2009 *Ortho–para* transition of interstitial H_2 and D_2 in Si. *Phys. Rev. B* **80**, 125207. (doi:10.1103/PhysRevB.80.125207)
69. Hourahine B, Jones R. 2003 Infrared activity of hydrogen molecules trapped in Si. *Phys. Rev. B* **67**, 121205. (doi:10.1103/PhysRevB.67.121205)
70. Klemperer W, Lehmann KK, Watson JKG, Wofsy SC. 1993 Can molecules have permanent electric dipole moments? *J. Phys. Chem.* **97**, 2413–2416. (doi:10.1021/j100112a049)
71. Fierz M. 1939 Über die relativistische Theorie kräftefreier Teilchen mit beliebigem Spin. *Helv. Phys. Acta* **12**, 3–37. (doi:10.5169/seals-110930)
72. Pauli W. 1940 The connection between spin and statistics. *Phys. Rev.* **58**, 716–722. (doi:10.1103/PhysRev.58.716)
73. Farkas A. 1935 *Orthohydrogen, parahydrogen and heavy hydrogen*. Cambridge, UK: Cambridge University Press.
74. Sandler YL. 1952 The *ortho–para* conversion of deuterium in molecular electric fields. *J. Chem. Phys.* **20**, 1050. (doi:10.1063/1.1700643)
75. Tikhonov VI, Volkov AA. 2002 Separation of water into its *ortho* and *para* isomers. *Science* **296**, 2363. (doi:10.1126/science.1069513)
76. Abragam A. 1961 *The principles of nuclear magnetism*. Oxford, UK: Clarendon Press.
77. Levitt MH. 2007 *Spin dynamics*. *Basics of nuclear magnetic resonance*, 2nd edn. Chichester, UK: Wiley.
78. Kellogg JMB, Rabi II, Ramsey NF, Zacharias JR. 1939 The magnetic moments of the proton and the deuteron. The radiofrequency spectrum of H_2 in various magnetic fields. *Phys. Rev.* **56**, 728–743. (doi:10.1103/PhysRev.56.728)
79. Brown JM, Carrington A. 2003 *Rotational spectroscopy of diatomic molecules*. Cambridge, UK: Cambridge University Press.
80. Quinn WE, Baker JM, LaTourrette JT, Ramsey NF. 1958 Radio-frequency spectra of hydrogen deuteride in strong magnetic fields. *Phys. Rev.* **112**, 1929–1940. (doi:10.1103/PhysRev.112.1929)
81. Ramsey NF. 1952 Theory of molecular hydrogen and deuterium in magnetic fields. *Phys. Rev.* **85**, 60–65. (doi:10.1103/PhysRev.85.60)
82. Hubbard PS. 1963 Theory of nuclear magnetic relaxation by spin–rotational interactions in liquids. *Phys. Rev.* **131**, 1155–1165. (doi:10.1103/PhysRev.131.1155)
83. Cohen-Tannoudji C, Diu B, Laloë F. 1977 *Quantum mechanics*. London, UK: Wiley.
84. Yildirim T, Harris AB. 2002 Rotational and vibrational dynamics of interstitial molecular hydrogen. *Phys. Rev. B* **66**, 214301. (doi:10.1103/PhysRevB.66.214301)
85. Mamone S, Pileio G, Levitt MH. 2010 Orientational sampling schemes based on four dimensional polytopes. *Symmetry* **2**, 1423–1449. (doi:10.3390/sym2031423)
86. Rafailov PM, Thomsen C, Bassil A, Komatsu K, Bacsa W. 2005 Inelastic light scattering of hydrogen containing open-cage fullerene ATOCF. *Phys. Stat. Sol. b* **242**, R106–R108. (doi:10.1002/pssb.200541168)
87. Hunt JL, Welsh HL. 1964 Analysis of the profile of the fundamental infrared band of hydrogen in pressure-induced absorption. *Can. J. Phys.* **42**, 873–885. (doi:10.1139/p64-082)

Downloaded from rsta.royalsocietypublishing.org on August 12, 2013

88. Hourahine B, Jones R, Öberg S, Newman RC, Briddon PR, Roduner E. 1998 Hydrogen molecules in silicon located at interstitial sites and trapped in voids. *Phys. Rev. B* **57**, R12 666–R12 669. (doi:10.1103/PhysRevB.57.R12666)
89. De Kinder J, Bouwen A, Schoemaker D. 1995 Molecular hydrogen in porous Vycor glass. *Phys. Rev. B* **52**, 15 872–15 880. (doi:10.1103/PhysRevB.52.15872)
90. FitzGerald SA, Forth S, Rinkoski M. 2002 Induced infrared absorption of molecular hydrogen in solid C_{60}. *Phys. Rev. B* **65**, 140302. (doi:10.1103/PhysRevB.65.140302)
91. Chen JYC, Martí AA, Turro NJ, Komatsu K, Murata Y, Lawler RG. 2010 Comparative NMR properties of H_2 and HD in toluene-d_8 and in H_2/HD@C_{60}. *J. Phys. Chem. B* **114**, 14 689–14 695. (doi:10.1021/jp102860m)
92. Li Y, Lei X, Lawler RG, Murata Y, Komatsu K, Turro NJ. 2011 Distance-dependent *para*-$H_2 \rightarrow$ortho-H_2 conversion in H_2@C_{60} derivatives covalently linked to a nitroxide radical. *J. Phys. Chem. Lett.* **2**, 741–744. (doi:10.1021/jz200192s)
93. Haupt J. 1972 A new effect of dynamic polarization in a solid obtained by rapid change of temperature. *Phys. Lett. A* **38**, 389–390. (doi:10.1016/0375-9601(72)90219-8)
94. Horsewill AJ. 1999 Quantum tunneling aspects of methyl group rotation studied by NMR. *Prog. NMR Spectrosc.* **35**, 359–389. (doi:10.1016/S0079-6565(99)00016-3)
95. Ludwig C, Saunders M, Marin-Montesinos I, Günther UL. 2010 Quantum rotor induced hyperpolarization. *Proc. Natl Acad. Sci. USA* **107**, 10 799–10 803. (doi:10.1073/pnas.0908421107)
96. Tomaselli M, Degen C, Meier BH. 2003 Haupt magnetic double resonance. *J. Chem. Phys.* **118**, 8559–8562. (doi:10.1063/1.1573635)
97. Tomaselli M. 2003 Dynamics of diatomic molecules in a chemical trap I. NMR experiments on hydrogen in solid C_{60}. *Mol. Phys.* **101**, 3029–3051. (doi:10.1080/00268970310001627431)
98. Tomaselli M, Meier BH. 2001 Rotational-state selective nuclear magnetic resonance spectra of hydrogen in a molecular trap. *J. Chem. Phys.* **115**, 11 017–11 020. (doi:10.1063/1.1429655)
99. Pake GE. 1948 Nuclear resonant absorption in hydrated crystals: fine structure of the proton line. *J. Chem. Phys.* **16**, 327. (doi:10.1063/1.1746878)
100. Fedders PA. 1979 Nuclear spin–lattice relaxation times for H_2 in solid nonmagnetic hosts. *Phys. Rev. B* **20**, 2588–2593. (doi:10.1103/PhysRevB.20.2588)
101. Mehring M. 1982 *High resolution NMR in solids*, 2nd edn. Berlin, Germany: Springer.
102. Hall DA, Maus DC, Gerfen GJ, Inati SJ, Becerra LR, Dahlquist FW, Griffin RG. 1997 Polarization-enhanced NMR of biomolecules in frozen solution. *Science* **276**, 930–932. (doi:10.1126/science.276.5314.930)
103. Ardenkjaer-Larsen JH, Fridlund B, Gram A, Hansson G, Hansson L, Lerche MH, Servin R, Thaning M, Golman K. 2003 Increase in signal-to-noise ratio of >10,000 times in liquid-state NMR. *Proc. Natl Acad. Sci. USA* **100**, 10 158–10 163. (doi:10.1073/pnas.1733835100)
104. Bowers CR, Weitekamp DP. 1986 Transformation of symmetrization order to nuclear-spin magnetization by chemical reaction and nuclear magnetic resonance. *Phys. Rev. Lett.* **57**, 2645–2648. (doi:10.1103/PhysRevLett.57.2645)
105. Bowers CR, Weitekamp DP. 1987 Parahydrogen and synthesis allow dramatically enhanced nuclear alignment. *J. Am. Chem. Soc.* **109**, 5541–5542. (doi:10.1021/ja00252a049)
106. Adams RW *et al.* 2009 Reversible interactions with para-hydrogen enhance NMR sensitivity by polarization transfer. *Science* **323**, 1708–1711. (doi:10.1126/science.1168877)
107. Levitt MH. 2012 Singlet nuclear magnetic resonance. *Annu. Rev. Phys. Chem.* **63**, 89–105. (doi:10.1146/annurev-physchem-032511-143724)